HERBIG-HARO FLOWS

BO REIPURTH
Center for Astronomy and Space Astrophysics
University of Colorado
Boulder, CO 80309, USA

AND

A.C. RAGA
Instituto de Astronomía
UNAM, Ap. 70-264, 04510 DF
México

1. Introduction

In the course of objective prism surveys of dark clouds, Herbig (1950, 1951, 1952) and Haro (1952, 1953) discovered a number of small objects, which display characteristic emission line spectra of hydrogen and forbidden low excitation lines of mainly [OI], [NII] and [SII], with at most very weak continua. On direct photographic plates, Herbig and Haro found these objects to be tiny, almost semi-stellar nebulae, with a tendency to be located in groups, often aligned in strings of objects. Ambartsumian (1954) subsequently coined the term Herbig-Haro objects for these tiny nebulae. From their location in dark clouds often containing nebulous stars or the newly recognized T Tauri stars (cf. Joy 1942, Ambartsumian 1947), early researchers concluded that the HH objects were somehow related to the process of star birth.

2. Herbig-Haro Objects at Different Wavelengths

2.1. OPTICAL SPECTRA

One of the brightest known HH objects, HH 1, has been the subject of the most detailed spectroscopic studies up to now. Its spectrum was first described by Herbig (1951), and subsequent spectrophotometric studies (e.g. Böhm 1956, Osterbrock 1958, Haro & Minkowski 1960, Böhm *et al.* 1973)

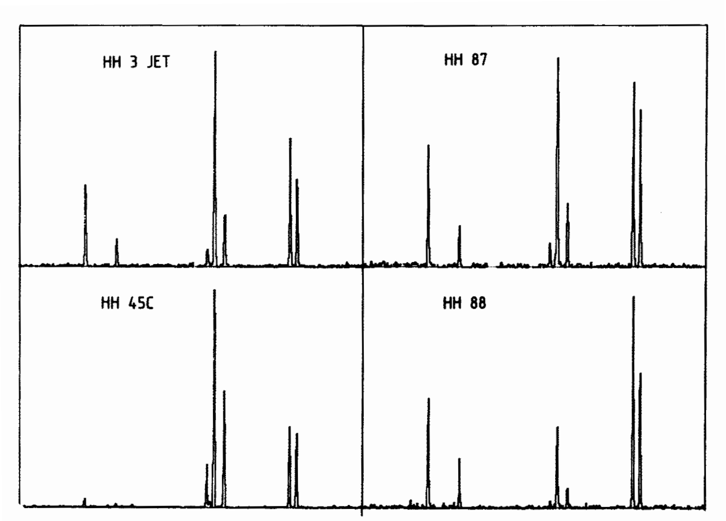

Figure 1. *Low resolution spectra of four HH objects, showing the large variation of emission line strengths. The lines seen are [OI] 6300, [OI] 6363, [NII] 6548, Hα, [NII] 6584, [SII] 6717 and [SII] 6731. From Reipurth (1989b).*

further established its peculiar nature. In an HH object, permitted and forbidden emission from neutral atoms (e.g. [OI], OI, [CI], [NI]) and from ions of low ionization energy (e.g. CaII, [CaII], [FeII], MgII, [SII]) are much stronger than in common photo-ionized nebulae. However, line-ratios can vary greatly from one HH object to another, and HH objects are often classified according to their level of "excitation" (e.g. Böhm 1983). HH 1 is the prototype of a high excitation object: for example, its [SII]6717/Hα ratio is very low ($\sim$0.2), its [OIII]5007/Hβ ratio is high ($\sim$0.6), its [NI]5198/5200 to Hβ ratio is low ($\sim$0.2), and its [CI]9848/Hα ratio is very low ($\sim$0.02) (Brugel *et al.* 1981a, Solf *et al.* 1988). HH 7, on the other hand, is a typical low excitation object, with a very high [SII]6717/Hα ratio ($\sim$2.8), no detection of [OIII]5007, a very high [NI]5198/5200 to Hβ ratio ($\sim$1.8) and a very high [CI]9848/Hα ratio of $\sim$1.3 (Böhm *et al.* 1980, 1983). Most HH objects have line-ratios which lie within these values. Fig. 1 illustrates a variety of HH spectra in the region around Hα.

For a derivation of line-ratios, and a meaningful interpretation of them, HH spectra must be de-reddened. This correction can be significant, because HH objects mostly are located in regions of rather high extinction. The best method to correctly determine the reddening of an HH object is the one of Miller (1968). In this method, the sum of the auroral lines of [SII] at $\lambda\lambda$ 4068/4076 are compared with the sum of the transauroral lines of [SII] at $\lambda\lambda$ 10318/10337. These lines appear in very different parts of the spectrum, but originate from the same upper energy level. Their theoretical ratio is therefore fully determined by the ratios of their transition probabilities and their frequencies; but the observed ratio is additionally affected by reddening. Adopting an extinction curve then leads directly to an E(B–V) for the observed object. While easy in principle, in practice it is not trivial to get accurate, good signal-to-noise observations of the [SII] lines beyond 1 μm. Another similar method is to compare Balmer and Paschen lines which come from the same upper level; for a careful discussion of these reddening methods see Solf *et al.* (1988). For spectra that do not have sufficient spectral coverage to include both sets of lines, more indirect methods exist (e.g. Dopita 1978). In the near-infrared, the [FeII] lines at 1.64 and 1.25 μm also arise in the same upper level and have been used to infer reddenings in HH objects (e.g. Gredel 1994).

In addition to emission lines, HH objects have very weak continua (Herbig 1951, Böhm 1956, Böhm *et al.* 1974, Brugel *et al.* 1981b). Although in a few HH objects one observes red continua due to reflected light from the stellar energy source, the majority of continua are blue, and indeed keep rising into the ultraviolet. These blue continua were interpreted as the result of a collisionally enhanced two photon decay mechanism in neutral atomic hydrogen by Dopita *et al.* (1982a) and Brugel *et al.* (1982). High signal-to-noise data for HH 1 corroborate this suggestion (Solf *et al.* 1988).

An important step towards interpreting the spectra of HH objects came with the realization that their line spectra could originate in the cooling regions behind shock waves (Schwartz 1975, 1978). This was borne out in more detailed comparisons between observed line ratios and plane-parallel shock wave models (Dopita 1978, Raymond 1979). The best fits to the observed data came for shocks with velocities of typically $70 - 100$ km s^{-1} moving into a rather low density, almost neutral medium. However, none of the models could reconcile the simultaneous presence of low excitation lines of [OI] and [SII] with highly ionized species like CIV. The introduction of bow shock models has resolved many of the inconsistencies inherent in the plane-parallel shock geometry. A bow shock produces a range of shock velocities, because only the component of the flow velocity perpendicular to the bow shock is thermalized. A single bow shock can therefore produce high excitation near its apex and simultaneously much lower excitation lines from the oblique shocks along its wings (e.g. Hartmann & Raymond 1984, Choe *et al.* 1985, Raga & Böhm 1985, 1986, Hartigan *et al.* 1987, Raymond *et al.* 1988).

The relevance of bow shock models for HH objects is supported not only by the line ratios they produce, but also by the line shapes they predict. The kinematics of the flow in the recombination region behind the shock can be

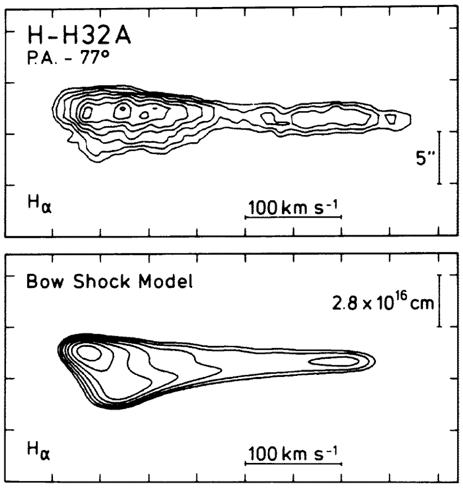

Figure 2. An observed Hα long slit spectrum of HH 32A and the predicted position-velocity diagram from a bow shock model. From Solf et al. (1986).

accurately predicted, and by integrating the emission over an appropriate volume (e.g. corresponding to what is seen through a spectrograph slit) a direct comparison with observations can be made. The results can be presented either as line profiles (e.g. Hartigan *et al.* 1987, Raymond *et al.* 1988) or also including the spatial dimension as position-velocity diagrams (e.g. Choe *et al.* 1985, Raga & Böhm 1985, 1986, Hartigan *et al.* 1990).

Fig. 2 shows a comparison of the observed long-slit spectrum of the Hα line in HH 32A with a position-velocity diagram calculated to reproduce the observed features, from a detailed study of the HH 32 complex by Solf *et al.* (1986). On the spatial (vertical) axis, the source is located towards the bottom, and on the velocity (horizontal) axis lower (more negative) velocities are towards the left, and higher (more positive) velocities towards the right. The immediately striking feature of the observed line profile is its very large width, of more than 350 km s^{-1}. This can readily be reproduced by a bow shock because it, as distinct from a plane-parallel shock, contains a large range of velocities projected along the line of sight, in addition to the thermal broadening of the emission from the hot post-shock gas. The observed emission clearly has two peaks, which are rather well reproduced in the model; they arise from regions near the bow apex and from the bow wings, respectively. Finally, the line has a distinct triangular shape. This asymmetry is related to the angle under which the bow shock is observed: for a bow shock moving in the plane of the sky the line is completely symmetric, but for bow shocks moving at increasingly small angles to the line of sight the asymmetry becomes more and more pronounced (Raga & Böhm 1986, Hartigan *et al.* 1987). The angle of the flow is a parameter to which the models are very sensitive. The parameters which Solf *et al.* (1986) found best match the observation in Fig. 2 are: bow shock velocity 300 km s^{-1} at the stagnation point, and an angle to the line of sight of 20°, with the object moving away from the observer. Hartigan *et al.* (1987) present simple analytic formulae that can be used to estimate the shock velocity and bow shock orientation from a single high resolution spectrum of a low excitation line.

Ideally, spectroscopic observations should provide both the large spectral range needed to yield numerous line-ratios, and the high spectral and spatial resolution necessary to map the kinematics of the flow in each emission line (e.g. Solf *et al.* 1988, Böhm & Solf 1990, Solf & Böhm 1991). For further details on the optical emission line spectra of HH objects, see the reviews of Böhm (1990) and Böhm & Goodson (1997).

2.2. INFRARED SPECTRA AND IMAGES

The near-infrared spectral region contains a number of emission lines of molecular hydrogen, which have proven to be important diagnostics for the molecular component of the gas in HH objects. The strongest and most commonly studied line is the 2.12 μm $v = 1 - 0$ S(1) line of H_2. This line was first detected in HH objects around T Tauri by Beckwith *et al.* (1978). Elias (1980) detected the line in a number of southern HH objects, and from a study of line-ratios concluded that the molecular gas was dense ($\sim 10^4$ cm^{-3}) and heated by shock waves. It is now clear that molecular hydrogen can contribute sometimes significantly to postshock cooling, and that shock-codes should incorporate both atomic and molecular processes. A considerable fraction of the HH objects detected have low-excitation optical spectra formed in low velocity or oblique shocks.

Near-infrared imagers and spectrographs have now reached such a level of development that it is possible to study the morphology and line strengths of the infrared emission from a large number of HH flows, particularly the strong and abundant infrared lines of H_2. Additionally, spectra in the H-band will record the [FeII] lines at 1.64 μm and 1.25 μm, which both arise from the same upper level, and therefore can be used to derive the reddening in an HH flow. [FeII] lines are also useful indicators of electron density.

The ground state of H_2 has many vibration-rotation levels with excitation energies from less than 1000 K to several times 10000 K. The resulting lines are likely to be collisionally excited in shocked gas with temperatures of a few thousand degrees, as originally discussed by Elias (1980). Such thermal excitation will populate only the lowest vibrational levels (v$\leq$3). Other non-thermal mechanisms have been discussed as well, particularly excitation due to fluorescence pumped by UV photons. Such processes will populate also high (v>3) vibrational levels. High signal-to-noise spectra of spectral regions where higher vibrational level lines should appear are therefore important in order to distinguish between thermal and non-thermal excitation mechanisms.

A convenient way of presenting the information of molecular hydrogen spectra is the H_2 excitation diagram, in which a measure of population density is plotted against excitation energy of the upper level for each transition. Gredel (1994) discusses the underlying physics, here it suffices to say that if the emitting gas can be characterized by a single temperature then the data points will fall along a straight line, with a slope proportional to the inverse of the excitation temperature. But if the emission comes from gas at a range of temperatures, then the line will be curved.

Gredel (1994) has obtained relatively high resolution infrared spectra of a large number of HH flows. For all of the objects, he finds a thermal population distribution which can be described by single excitation temperatures in the range from 2000 K to 2700 K. Fig. 3 shows in panel A the K-band spectrum of HH 43, one of the brightest H_2 emitters among HH objects, in panel B the H-band spectrum, and in panel C the resulting excitation diagram. Gredel derives an excitation temperature for HH 43 of 2200 K. In the H-band spectrum there should be five (6,4) Q(1)-Q(5) lines in the 1.60 to 1.64 μm region if any non-thermal emission was present. None are seen. There *is* in fact fluorescently excited H_2 in HH 43, but it has so far only been detected in the UV, where Schwartz (1983) observed eight Lyman band emission lines between 1250 Å and 1600 Å.

Both C-type (continuous) and J-type (jump shocks) have been invoked to explain the infrared line spectra in HH flows. C-shocks require a magnetized medium of low ionization (e.g. Smith 1993). J-shocks require a medium of higher ionization that is not so strongly magnetized (Smith 1994a). The intensities in the (1,0) S(1) H_2 line that Gredel (1994) observed in various HH objects can be produced by slow non-dissociative J-shocks. The observed intensities of the [FeII] 1.64 μm line are, on the other hand, well modelled by fast, dissociative J-shocks in the 40-60 kms^{-1} range. This can be reconciled only if the H_2 and [FeII] emission originate in separate regions, and Gredel (1994) suggests that curved bow shocks of J-type could explain the data, with the [FeII] emission arising in the fast, dissociative region near the apex of the bow shock, and the H_2 emission in the slower, non-dissociative wings. Schwartz et al. (1995) arrive at similar conclusions.

The similarities and differences between distributions of optical and molecular shock regions may also provide essential clues to the flow struc-

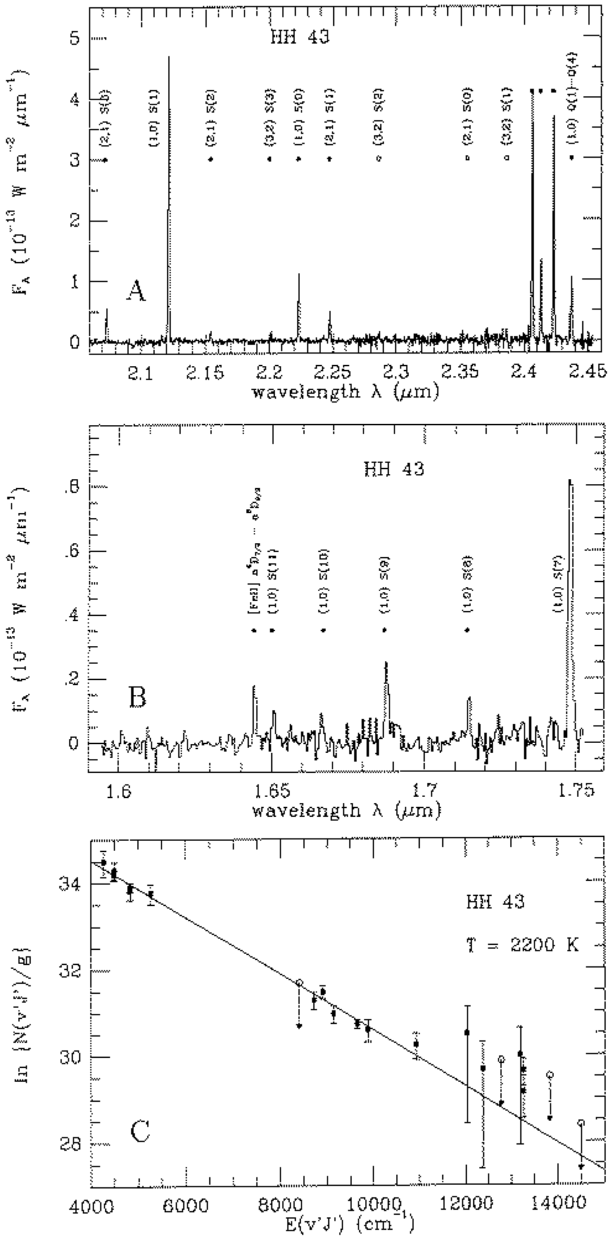

Figure 3. Infrared spectroscopy of HH 43. Panel A shows a K-band spectrum, and Panel B an H-band spectrum. Panel C shows the resulting H_2 excitation diagram. From Gredel (1994).

ture in HH objects. Such studies have been performed by e.g. Schwartz *et al.* (1988), Hartigan *et al.* (1989), Garden *et al.* (1990), Wilking *et al.* (1990), Zealey *et al.* (1992), Carr (1993), Eislöffel *et al.* (1994b), Davis *et al.* (1994), Gredel & Reipurth (1994). It appears that the H_2 emission occurs mainly in the wings of the bow shocks, where the shocks are oblique and thus much weaker.

2.3. ULTRAVIOLET SPECTRA

It came as a surprise when Ortolani & D'Odorico (1980) discovered a strong continuum and emission lines in the ultraviolet spectrum of HH 1, considering its not insignificant reddening. Subsequently, more than a dozen studies of ultraviolet spectra of HH objects have confirmed the importance of UV radiation from these objects.

The UV spectra of high-excitation objects are dominated by emission lines of [CIV] 1548/1551 and [CIII] 1907/1909; low-excitation objects, on the other hand, almost exclusively show fluorescent lines of the Lyman bands of the H_2 molecule (Schwartz 1983). The UV continuum rises towards shorter wavelengths, particularly rapidly between 1700Å and 1620Å, with a peak around 1575Å. This continuum is likely to be a continuation of the observed blue continuum, and is also believed to be due to a collisionally enhanced two photon decay mechanism in neutral atomic hydrogen (Brugel *et al.* 1982), but an additional component due to fluorescent H_2 appears to play a role at the shortest wavelengths (Böhm *et al.* 1987).

Interpretations of UV observations are extremely sensitive to the reddening corrections applied. Although the amount of extinction can be reasonably determined using the Miller (1968) method, the shape of the extinction curve may differ from region to region. Böhm-Vitense *et al.* (1982) argued that flatter than normal extinction curves (like the θ Ori curve) may be appropriate, though this result was partially called into question by Böhm et al. (1991).

All the brightest HH objects have now been observed in the UV (Brown *et al.* 1981; Böhm *et al.* 1981, Böhm & Böhm-Vitense 1984; Brugel *et al.* 1985; Schwartz *et al.* 1985; Noriega-Crespo *et al.* 1989, Cameron & Liseau 1990, Böhm *et al.* 1993, Liseau *et al.* 1996 and Hartigan *et al.* 1999; and above mentioned references).

3. Morphological and Kinematic Properties of Jets

A particularly intriguing subset of Herbig-Haro objects is formed by the highly collimated HH jets (Fig. 4 and Fig. 5). The first jet recognized as such was the HH 47 jet (Dopita *et al.* 1982b), which remains one of the finest cases known. Mundt & Fried (1983) and Mundt *et al.* (1983, 1984) did

CCD imaging of young stars and known HH objects and discovered several more HH jets. A large number of detailed studies of HH jets now exists in the literature, e.g. Graham & Elias (1983), Reipurth *et al.* (1986), Mundt *et al.* (1990, 1991), Reipurth & Heathcote (1991), Eislöffel *et al.* (1994a), Bally *et al.* (1995), Heathcote *et al.* (1996), Reipurth *et al.* (1997a).

The opening angle of jets are in general small, of the order of a few degrees. Length-to-width ratios vary considerably, from fairly poorly collimated jets with a ratio of 5 or so to extremely high ratios exceeding 100 (e.g. HH 333; Bally *et al.* 1996). The widths of jets are mostly poorly determined, but are in a few cases known well; the HH 34 jet for example has a width of 0.7 arcseconds or 300 AU (Raga & Mateo 1988, Bührke *et al.* 1988, Raga *et al.* 1991b) and a width of about 0.8 arcseconds was found for HH 111 (Reipurth *et al.* 1992, 1997a).

All jets have a knotty sub-structure, with typical semi-regular spacings of one to a few arcseconds. These knots do not always trace a perfectly straight line, in fact it is common for jets to show considerable wiggling. The knots provide a means to measure transverse motions of jets; proper motions have been measured quite accurately for many jets by now, and typical transverse motions are around 200$-$300 km s^{-1} (e.g. Herbig & Jones 1981, 1983, Heathcote & Reipurth 1992, Eislöffel *et al.* 1994a).

In many cases HH jets are bipolar, tracing an approaching and a receding lobe. The two lobes are generally very asymmetric, usually due to uneven obscuration. However, cases exist where the asymmetries appear to be real, either because the jet-flow is intrinsically asymmetric, or because of differences in the ambient medium into which the jets flow (e.g. Mundt *et al.* 1987, Hirth *et al.* 1994, Reipurth *et al.* 1998a).

Long slit spectra along a jet axis give information on the variation of the radial velocity, line width, excitation and electron density in the flow. Such studies have now been made for many jets, see for example Solf (1987), Meaburn & Dyson (1987), Solf & Böhm (1987), Mundt *et al.* (1987), Bührke *et al.* (1988), Reipurth (1989a,b), Mundt *et al.* (1990), Hartigan *et al.* (1990), Heathcote & Reipurth (1992), Solf & Böhm (1993). Typical radial velocities are high, around $100 - 200$ km s^{-1}. Jets show velocity variations, which are often complex but rarely major. When an ordered motion is found it is mostly a decrease in the radial velocity; in one case, HH 83, a major increase in radial velocity is measured as one moves away from the source (Reipurth 1989b).

Electron densities as derived from the [SII] 6717/6731 ratio vary considerably, with values ranging typically from a few hundred to a few thousand electrons per cm^3. When changing systematically along the jet, the electron density more often decreases, which in the simplest interpretation suggests diverging flows (e.g. Mundt *et al.* 1987). It is not so easy to determine the

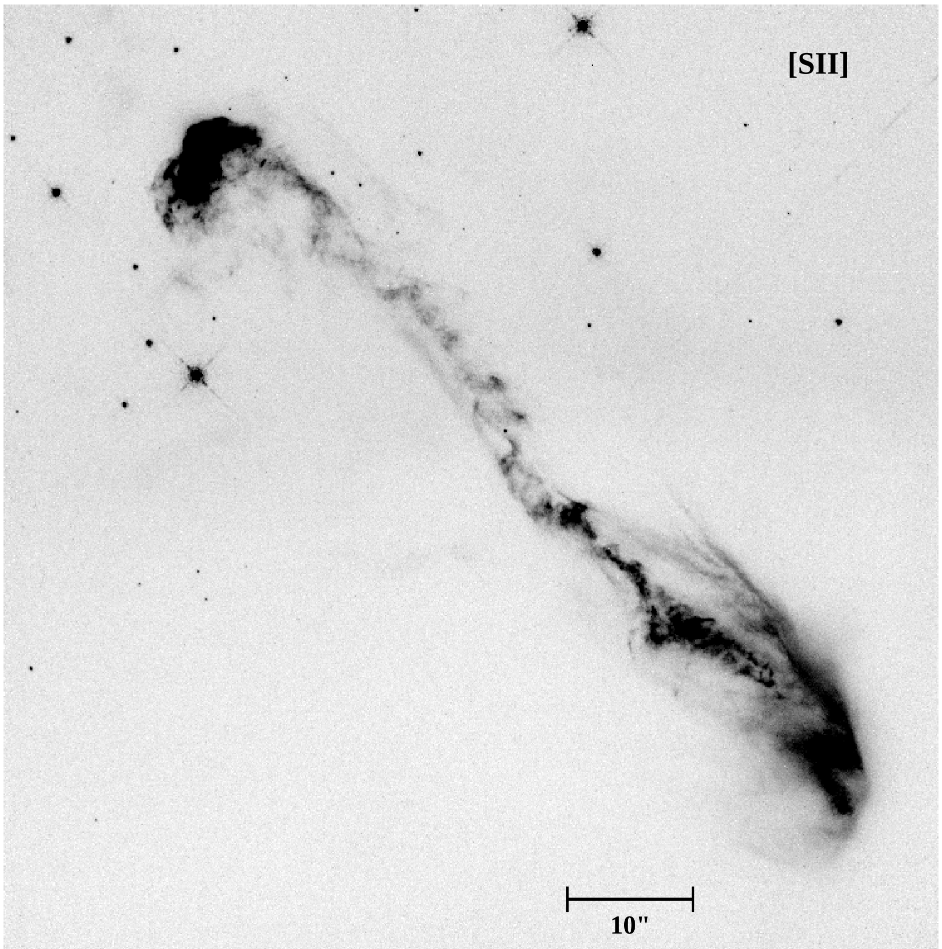

Figure 4. *A [SII] image of the HH 47 jet obtained with WFPC2 at HST. The jet emerges from a Bok globule in the Gum Nebula, and is powered by an embedded IRAS source located near the lower right hand corner of the image. The source illuminates the walls of a cavity through which the jet emerges, producing a bright reflection nebula, which curves around and above the beginning of the jet. The body of the jet, which is very bright in [SII], consists of a sinuous chain of knots. The jet ends in a bright, extended working surface, HH 47A, surrounded by a faint veil that sweeps backwards. At this point, jet material is shocked and decelerated, while ambient material is shocked and accelerated. HH 47A is not the terminal working surface, as at least one more bow shock is known further out along the jet axis. The jet is not flowing along the complicated path seen here, rather, the meandering structure most probably reflects a wandering of the ejection axis near the source. From Heathcote et al. (1996).*

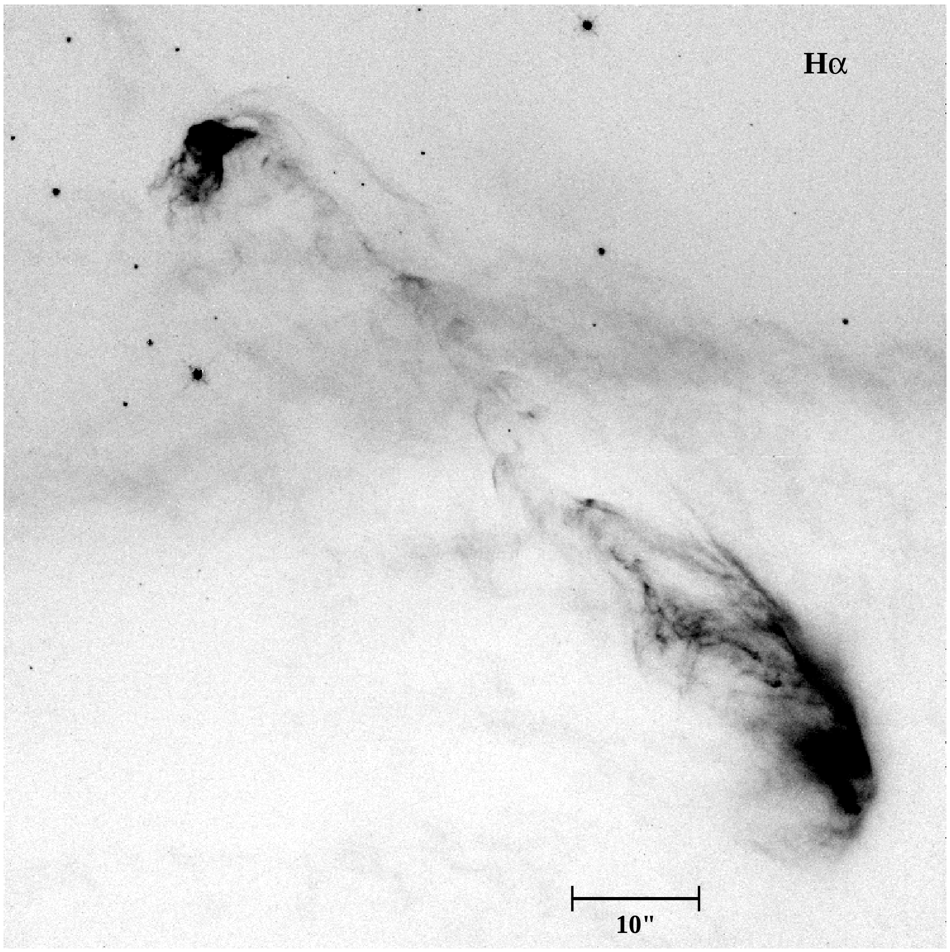

Figure 5. *An Hα image of the HH 47 jet obtained with WFPC2 at HST. The winding chain of knots seen in [SII] is here replaced with a delicate tracery of narrow filaments and wisps, with trailing wings swept back at an oblique angle to the flow direction. It turns out that the [SII]-bright knots delineate the "core" of the jet, while the Hα emission comes predominantly from the zone along the edges of the jet. The Hα wisps appear to resemble one-sided bow shocks that extend into and accelerate the ambient medium. This is consistent with kinematic studies which show that the core of the jet moves faster, and the edges slower. Entrainment and acceleration of the medium through which the jet flows thus occur both at the working surface of the jet and also along the body of the jet. The result is a molecular outflow which can be detected at millimeter wavelengths. From Heathcote et al. (1996).*

actual gas density of jets, because they have rather low ionization fractions, so that the gas number density is normally considerably larger than the observed electron density. In the model calculations of Raga *et al.* (1990b), the hydrogen ionization fraction is found to be at most 10%. Bacciotti et al. (1995) have suggested a line ratio analysis useful for determining the ionization fraction of HH objects, but the uncertainties involved are quite large (due to the strong temperature dependence of the line ratios).

The excitation of jets is generally low, and jets are normally prominent in CCD images obtained through a [SII] filter, and much weaker in Hα images. The low excitation character of HH jets and their very high space motions would appear contradictory, but could be reconciled either if the shocks in jets are very oblique (see e.g. Raga 1989), or, as we believe now, are due to small velocity variations along the flow axes (Raga *et al.* 1990a).

The velocity dispersions in HH jets are, with some exceptions, generally low or moderately low. In HH 34, for example, the widths of the [SII] 6717/6731 lines are less than 30 km s^{-1} (Bührke *et al.* 1988). In several jets, one sees a splitting of the lines, e.g. in HH 24 (Solf 1987), in HH 46/47 (Meaburn & Dyson 1987), in HH 34 (Bührke *et al.* 1988, Heathcote & Reipurth 1992) and in several jets in the HL Tau region (Mundt *et al.* 1990). In HH 24, Solf (1987) found two velocity components close to the source, a high velocity component displaying a gentle velocity decrease away from the source, and a weaker lower velocity component with a steep acceleration. Solf (1987) interprets this in terms of a jet model with an inner cylindrical core region and a co-axial envelope. The inner high velocity core is the jet itself and the envelope is ambient material dragged along with the jet; their mutual interaction will slightly slow down the jet and accelerate the entrained material. Using Fabry-Perot observations, Hartigan *et al.* (1993) directly showed how low-velocity gas in the HH 47 jet is surrounding the inner high-velocity gas, similar to a viscous flow in a pipe. The interaction of jets with their ambient medium is generally assumed to be the driving mechanism of the ubiquitous molecular outflows (see the chapter by Bachiller in these proceedings).

4. The HH 111 Jet Complex

One of the finest collimated HH jets is the HH 111 jet in Orion. It emerges from a dense cloud core in the L1617 cloud, which harbors a 25 L$_\odot$ infrared source (Reipurth 1989a). Fig. 6 shows the complex in a large field CCD image. The energy source, a class I source in the classification scheme of Lada (1987), is located at the center of the cloud core, which is outlined by faint Hα emission caused by the OB stars in the Ori Ib association. Light from the source illuminates a conical reflection nebula through which the jet emerges. The flow terminates in a bow shock (V) 142 arcseconds from the source, corresponding to 0.32 pc in projection. On the opposite

Figure 6. A red broadband CCD mosaic of the HH 111 jet complex, from the ESO 3.6m telescope. The jet emerges from an IRAS source embedded in a cloud core outlined by faint bright rims. Several bow shocks (V, L, X, Y) can be seen on either side of the cloud core. A bright knot (Z) in a very faint counter jet is also visible. From Reipurth et al. (1992).

side of the source, at a separation of 200 and 226 arcsec, respectively, two other bow shocks are found. The total extent of this complex is more than 0.8 pc in projection (as discussed later, the HH 111 flow actually extends much further than this). Spectroscopic observations show moderate radial velocities, with the western lobe containing the jet which approaches us, while the eastern lobe is receding. Proper motions have been determined for the flow, they are large, of the order of 300 km s^{-1} and directed away from the source (Reipurth *et al.* 1992). Fig. 7 shows the intensity profile of the jet in two Hα images, from 1987 and 1990; the shift due to the proper motion is obvious. From the proper motion and radial velocities one can derive an inclination of the jet to the plane of the sky of only about 10°.

The jet is very bright in [SII], suggesting that the shocks are weak. From the [SII] lines the electron density can be determined, and it is found to decrease steeply with distance from the source, which in the simplest interpretation suggests a constant mass flow through a slightly widening channel. But the electron density derived from the [SII] lines refers to the recombination region in the post-shock gas. Although a simple relation exists between pre-shock and post-shock density as a function of shock velocity (Dopita 1978), a jet consists of many shocks, and so the density may become a complex function of the flow geometry.

The HH 111 jet has been the subject of a very detailed study based on deep images in Hα and in [SII] obtained with WFPC2 onboard the Hubble Space Telescope (Reipurth et al. 1997a). The HST images of the almost perfectly straight HH 111 jet offer an unprecedented opportunity for studying the HH jet phenomenon. At the distance of Orion, a WFPC2

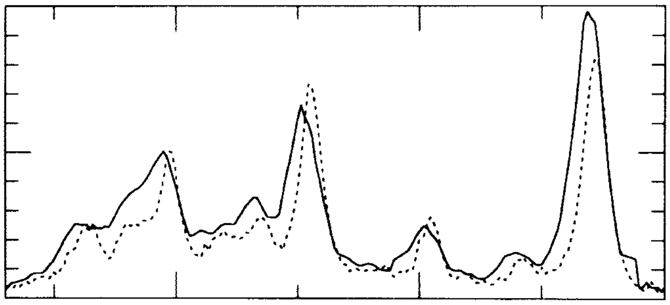

Figure 7. *Intensity profile of the HH 111 jet in Hα, observed in 1987 (full line) and in 1990 (dotted line). The driving source is towards the left. The proper motion of individual knots is clearly visible. From Reipurth et al. (1992).*

pixel of 0.1 arcsecond corresponds to 46 AU.

Figure 8 shows the HST images in Hα, [SII] and H$\alpha-$[SII] of the leading working surface V. This working surface is composed of two brightly emitting regions in Hα and in [SII] (Figure 8a and b), which are displaced from each other, forming a bow shock (forward shock) and Mach disk (reverse shock or jet shock), as can be seen in the H$\alpha-$[SII] image in Figure 8c. Closer examination of the Hα image reveals that the brightest emission comes from a very thin filament, unresolved even with HST, which curves around the very front of the bow shock. The filament itself does not emit in [SII], which only appears about $0.5''$ upstream. This feature is interpreted as a layer where neutral hydrogen atoms are collisionally excited thus giving rise to strong Balmer emission (Chevalier & Raymond 1978). The [SII] emission arc immediately behind the collisionally excited Hα filament arises in the resolved cooling zone, where gas heated in the forward shock cools and recombines, emitting forbidden metallic lines and Balmer emission.

Contour plots of the Hα and [SII] HST images of the HH 111 jet body are shown in Figure 9. These images provide a wealth of new information on the jet structure. The jet appears to be fully resolved perpendicular to the flow direction, and the knotty substructure is rich and complex. Knot L has the morphology of a well-defined bow shock, best seen in the Hα image. In the body of the jet, most of the brighter knots also have bow shock shapes, with a compression in the contours in the flow direction. Bow shock wings sweep backwards on either one or both sides of the bright knots. The fainter knots, on the other hand, have no characteristic structure.

In most places the jet is much brighter in [SII] than in Hα. Morphologically it is also different in the two lines: seen at lower light levels the jet knots are more distinct in Hα, whereas in [SII] the knots appear to be surrounded by a sheath of faint, diffuse emission. The brightest portion of

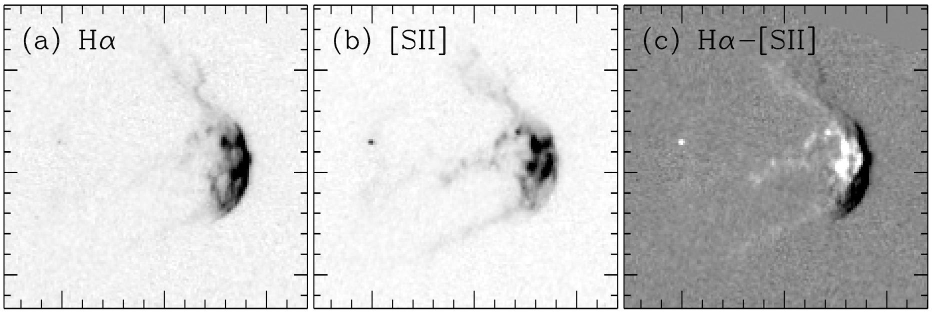

Figure 8. The HH 111V working surface as seen with HST: (a) Hα; (b) [SII]; and (c) an Hα−[SII] difference image in which Hα-bright regions are black and [SII]-bright regions are white. From Reipurth & Heathcote (1997).

this [SII] tube wavers from side to side as it follows behind the Hα emission, but, as discussed in more detail by Reipurth et al. (1997a), there is no evidence that the jet flow actually spirals about its axis.

Apart from the bright bow shocks L and E, the jet maintains a fairly constant width along its axis. The width of the jet body, measured by collapsing the jet between (and excluding) L and E and measuring the FWHM of the result, is 0.8 arcsec, both in [SII] and in Hα. However, it should be kept in mind that it is difficult to characterize a structure as complex as the HH 111 jet body with a single number. Figure 9 gives the impression that the jet becomes narrower between knots H and L, but this appearance simply results from the jet being fainter in this region.

Even higher resolution observations have been performed of the region of the embedded energy source, using the VLA in the A configuration at 3.6 cm (Rodríguez & Reipurth 1994). The source is detected as a relatively bright (0.9 mJy) object at 3.6 cm, and is shown in Figure 10 with a resolution of about 0.2 arcsec. The source clearly consists of a core with a one-sided radio jet extending towards the West at exactly the position angle of the optical jet. The angular "width" of the radio jet, 0.1 arcsec, is much smaller than the width of the optical jet, $\sim$0.8 arcsec. The ionized gas that emanates from the exciting star is very young: assuming a jet velocity of 320 kms^{-1} from the optical observations suggests an age of only a few years. The HH 111 energy source is thus at the very moment actively forming the jet.

5. Giant Herbig-Haro Jets

Until recently, the dimensions of HH flows have generally been assumed to be about a few arcminutes, which at a distance of, say, Orion corresponds to a fraction of a parsec, typically about 0.3 pc. A few flows were known with

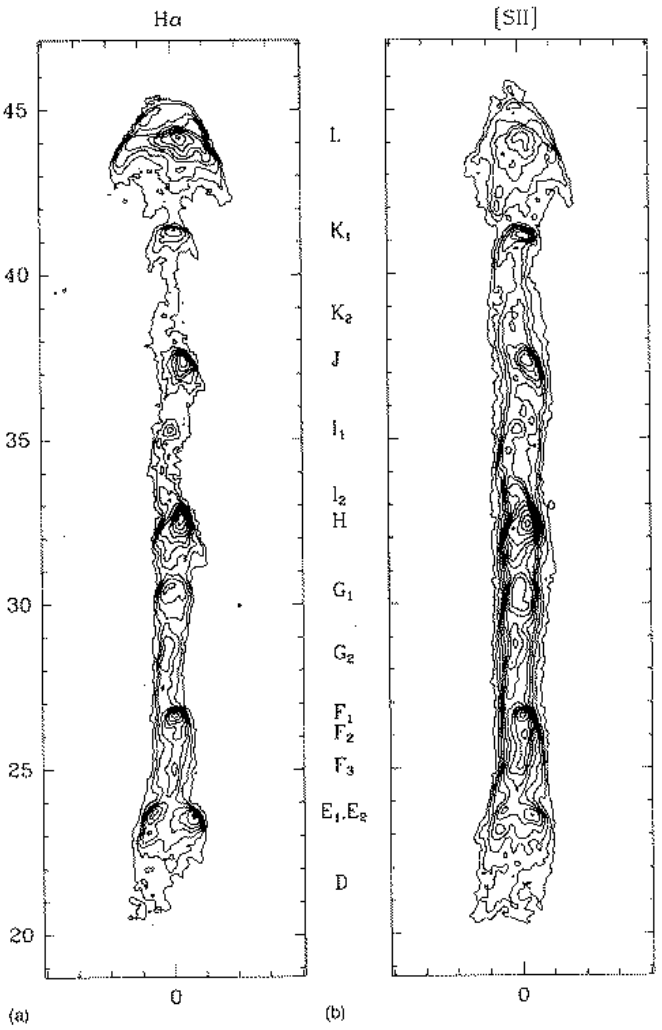

Figure 9. Contour plots of HST images of the HH 111 jet in Hα (left) and [SII] (right). From Reipurth et al. (1997a).

larger dimensions, but they were associated with more luminous stars. It is now of interest to note that the dimensions of a few arcminutes correspond well to the field size of the first few generations of CCD detectors. When Bally & Devine (1994) used a new wide field CCD imager in the HH 34 region, they saw faint emission features connecting the HH 34 complex with other HH regions previously assumed to be independent flows and all lying along a single well defined axis, and they realized that the HH

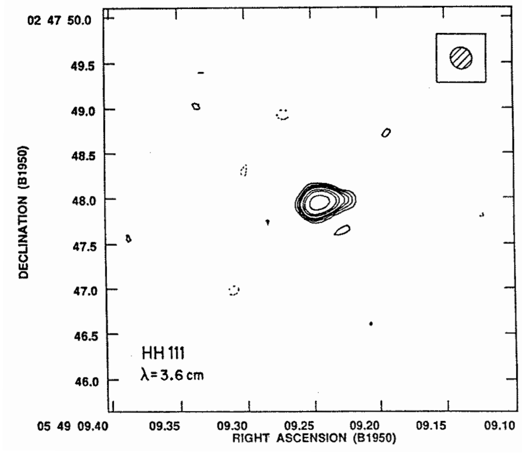

Figure 10. Cleaned natural-weight VLA-A map of the VLA source at HH 111 at 3.6 cm. Contours are -3, 3, 4, 5, 6, 8, 10, and 15 times 20 μJy beam^{-1}, the rms noise of the map. The half power contour of the beam is also shown. A small jet is seen to emanate in the direction towards the optical jet. From Rodríguez & Reipurth (1994).

34 flow stretches to HH 33/40 to the North and to HH 86-87-88 to the South, spanning 2.8 pc. In a detailed follow-up study, Devine *et al.* (1997) showed that all HH objects South of the HH 34 source are blueshifted and have proper motions to the South, while all HH objects to the North are redshifted and have proper motions to the North, thus establishing not only a positional and morphological link to the HH 34 source, but also a kinematical connection.

Following the recognition that HH flows from low mass stars can attain very large dimensions, a systematic survey for such giant flows was undertaken using large-field Schmidt films from the ESO Schmidt Telescope and large-field CCD images from CTIO and Kitt Peak. As a result, a large number of HH flows of gigantic proportions were discovered (Reipurth *et al.* 1997b, 1998b).

5.1. THE GIANT HH 111 JET COMPLEX

The HH 111 jet is the object which comes closest to the text book idealization of how a jet should look (see sect.4). Reipurth *et al.* (1997b) have demonstrated, on structural and kinematic grounds, that the HH 111 complex contains even more distant bow shocks, spanning 57 arcminutes, that is, almost a full degree on the sky; at a distance of 460 pc and inclined 10° to the plane of the sky, this corresponds to a physical extent of 7.7 pc.

The central panel in Figure 11 shows a [SII] CCD image of what we have

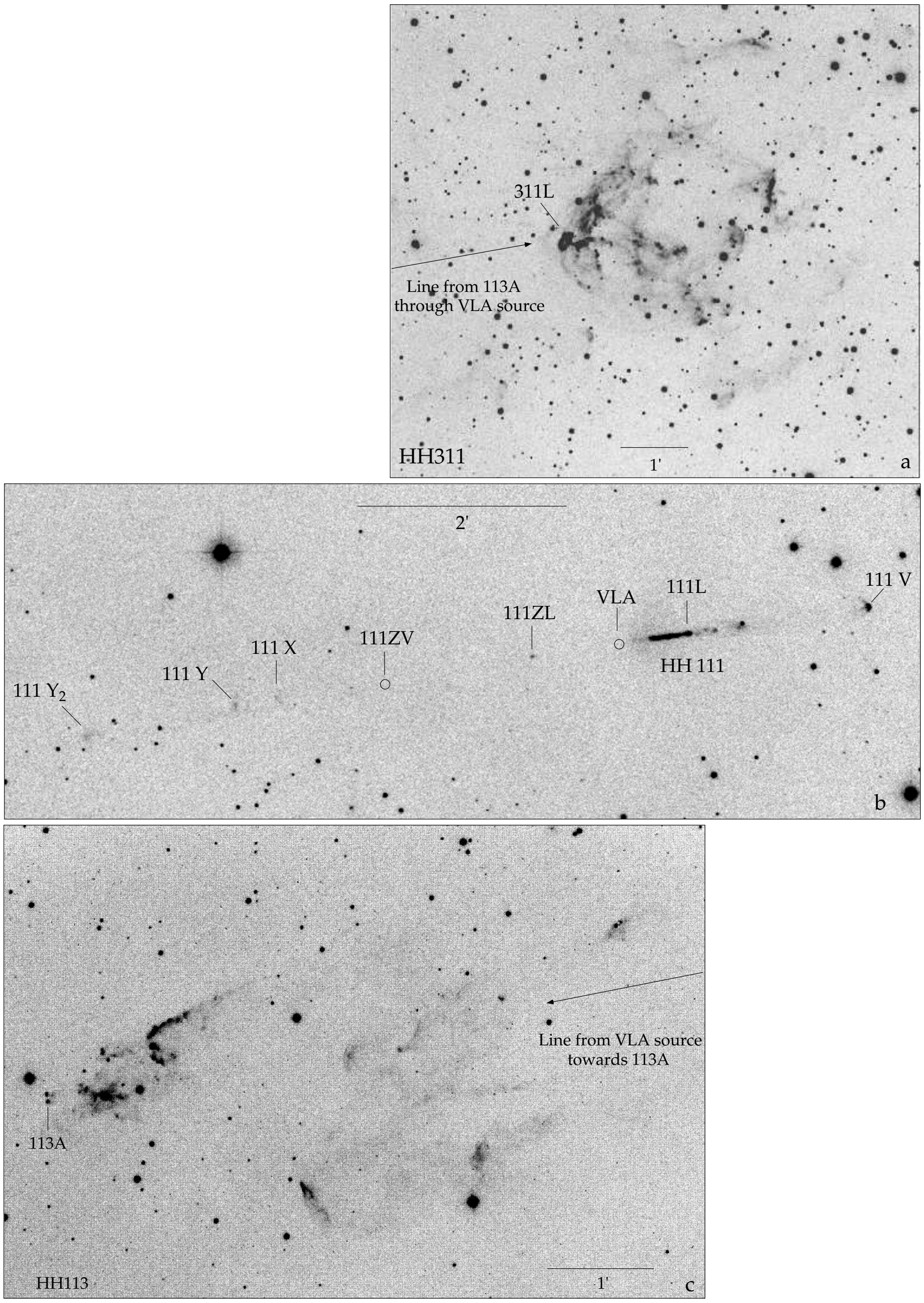

Figure 11. *A mosaic of the principal components of the giant HH 111 flow. From Reipurth et al. (1997b).*

up to now thought of as the HH 111 complex, from V to the West and to Y in the East. Another new knot, $111Y_2$, is also identified. If one moves further eastward, about 15 arcminutes from the VLA source, one finds another HH knot, $111Y_3$, on the well defined flow axis. Continuing another about 12 arcminutes to the East, one encounters the HH 113 complex. Based on small-field CCD images, Reipurth & Olberg (1991) considered this to be a separate HH flow, although they were puzzled about the absence of an energy source.

In the lower panel of Figure 11 we see new wide field Hα+[SII] images from the ESO New Technology Telescope. The HH complex appears to be a very large cone-shaped bow shock, with HH 113A at its apex. A line has been drawn pointing from the VLA source to the apex. The position angle of the line between the VLA source and the apex A is 101 degrees, only a few degrees larger than the values determined from the knots much closer to the source. It is remarkable that the flow can maintain such a directional stability over a length of 3.8 pc, which is the distance between the VLA source and knot A.

Precisely symmetrical with HH 113 around the VLA source, we find HH 311. The upper panel of Figure 11 shows the sum of Hα and [SII] images of HH 311 taken at the ESO NTT. The object is large, with a width and length of about 5 arcmin, corresponding to a projected size of 0.7×0.7 pc.

Multiple epoch CCD images of HH 113 and HH 311 have been obtained, from which proper motions have been derived. The principal knots in HH 113 are all moving towards the Southeast with velocities in the plane of the sky of order 50-150 $\mathrm{km\,s^{-1}}$, while knots in HH 311 are moving towards the Northwest with similar velocities. These proper motions provide very strong support for the idea that HH 113 and HH 311 form distant bow shocks in the HH 111 complex.

5.2. THE IMPORTANCE OF GIANT HH FLOWS

In their study, Reipurth et al. (1997b) discovered 9 HH flows with parsec-scale dimensions, and listed another 13 likely giant HH flows. The ubiquity of HH flows with such gigantic proportions has important consequences for our understanding of the HH phenomenon, as summarized in the following.

1. As the dimensions of HH flows increase by a factor of 5 or so, their dynamical ages increase by at least as much. In their detailed kinematical study of HH 34, Devine *et al.* (1997) demonstrated that the different components of the HH 34 giant flow decrease in space velocity linearly with distance from the source, as momentum is expended in pushing the flow through the interstellar medium. Alternatively, the observed velocity de-

crease with increasing distance from the outflow source could be the result of a gradual "turning on" of the jet flow at the beginning of its evolution. For the newly discovered giant flows, the dynamical ages of the most distant components are of the order of 10^4 - 10^5 years. The longer timescale is comparable to the stellar accretion phase and also to the lifetimes of molecular outflows estimated from millimeter observations.

2. Virtually all well developed jets have multiple working surfaces. This is also true on the larger scales of the giant HH flows, and it provides strong evidence for significant and periodic variability of the source on time scales of many hundred to several thousand years during the dynamical life time of the flow. When known, the space motions of the individual working surfaces exceed their shock velocities, implying that they are faster fluid elements overtaking slower moving material. It follows that most HH objects are internal shocks that define zones of interaction between material ejected at different times with different velocities.

3. Giant HH flows provide a record of the activity of the driving source on timescales significant compared to collapse time scales. Many parsec scale flows show s-shaped point symmetry around the source. This tells us that the axis of ejection is not stable, either because it precesses, or more likely because it wanders or wobbles under the erratic gravitational influence of forming and dissolving protoplanetary or protostellar condensations in its disk. Little more can be said about this influence until a clearer picture emerges of how jets are formed.

4. The behaviour of HH objects as they move away from their source is poorly understood, but from the currently available data it appears that HH objects gradually slow down with time, while at the same time their physical size increases, and they take increasingly chaotic shapes.

5. With sizes of several parsecs, HH flows can completely leave the parental cloud in which they formed and travel into the intercloud medium. One aspect of this is that newborn stars can inject energy and momentum into the interstellar medium far from their location. Another aspect is that terminal working surfaces of giant HH flows can be used as probes of the physical conditions in the surroundings of molecular clouds, because their physical and kinematical properties also depend on their environment.

6. When supersonic mass ejectae of HH flows encounter molecules in the ambient medium, the molecules can be dissociated, and thus the chemical abundances can be reset to values closer to the ones present at an earlier stage of the chemical evolution of the cloud (see, e. g., Charnley *et al.* 1988). They may have an effect on their environment which would be unexpected in the absence of UV radiation from massive stars. Finally they may contribute to the generation of turbulence in molecular clouds.

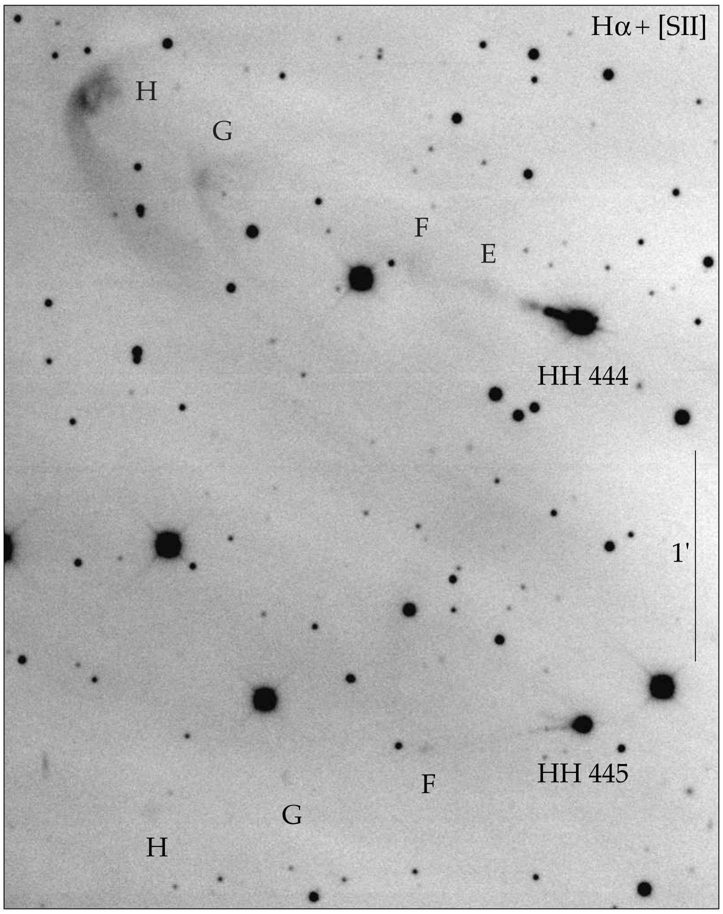

Figure 12. *Two irradiated jets, HH 444 and HH 445, located just East of the massive O-star σ Orionis. Both jets are subjected to and partially ionized by the strong UV radiation field of the O-star. From Reipurth et al. (1998a).*

6. Irradiated Jets

Most low-mass stars are born not in tranquil environments like the Taurus clouds or other T Tauri associations, but in dense clusters which include one or more massive OB stars. As a result, the young low-mass stars sooner or later become subjected to an intense UV irradiation, depending on when they were born relative to the appearance of the OB stars and on how soon their placental material is being eroded and swept away. This process may have important effects on the amount of material these stars have at their disposal for accretion, and thus it may affect the shape of the initial mass function in the cluster. It also has two effects related to the HH jets formed by these young stars. Firstly, the UV radiation may partly or fully ionize the jets themselves. HH jets normally emit through the shocks they produce, and a determination of the mass loss rate must therefore involve model dependent assumptions about the nature of the shocks. But if a jet becomes photoionized, it is possible to determine the density and mass flow much more directly and accurately. Secondly, the circumstellar material normally hiding the young star and its immediate surroundings is rapidly destroyed by the photo evaporation and photo ablation caused by the UV radiation of the nearby OB stars, and this opens the exciting possibility of examining the jet launch and collimation region of newborn stars, a region that has so far been largely excluded from observational scrutiny. Finally, a curious and unexpected result of the study of the more than a dozen irradiated jets known so far is that virtually all of these jets are one-sided or nearly one-sided. Whereas extinction is usually hiding one side of jets in more quiescent regions, this cannot easily be invoked for the highly exposed irradiated jets, and one is left to wonder if the strong UV radiation field may paly a role in this strong asymmetry. Altogether, the new study of irradiated jets may open up new approaches to the study of HH jets (Reipurth *et al.* 1998a).

7. Jets from Massive Stars

The jets and flows discussed so far have all emanated from low-luminosity low-mass stars. But a few HH flows from intermediate and higher mass stars have been found (e.g. Axon & Taylor 1984, Reipurth & Graham 1988, Ray *et al.* 1990, Poetzel *et al.* 1992, Ogura & Walsh 1992, Corcoran & Ray 1998, Devine *et al.* 1999).

HH 80/81 are the intrinsically brightest HH objects known, emanating from an embedded high-luminosity IRAS source (Reipurth & Graham 1988). The source is associated with a reflection nebula, GGD 27, and a large bipolar outflow, and is embedded in a dense flattened CS core (Yamashita *et al.* 1989). Compact radio continuum and H_2O maser emission was detected by Rodríguez *et al.* (1980), who suggested a distance of 1.7 kpc. At this distance HH 80/81 lie at a projected distance from the source of 2.3 pc.

Continuum observations of the region were made at 6 cm with the VLA–D array (Rodríguez & Reipurth 1989); both HH 80 and 81 were detected, and the central source was found to be significantly extended in the direction towards the HH objects. In three more recent studies Martí *et al.* (1993,1995,1998) used the VLA–A array to achieve maps of the region with a resolution of better than 1 arcsec. They found that the central source

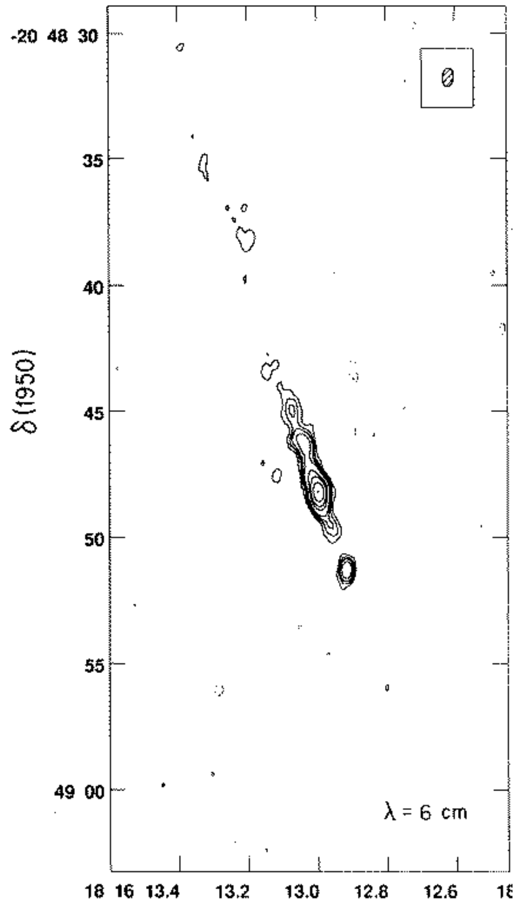

Figure 13. The highly collimated jet in the HH 80/81 complex. The central source is an 18000 $L_\odot$ B star, located in the bright central knot. The map is a 6 cm VLA map. At a distance of 1700 pc, 20 arcsecond correspond to 0.17 pc. From Martí et al. (1993).

powers a highly collimated bipolar radio jet, which shows high proper motions away from the source. The central region of the jet is shown in Fig. 13, it is unresolved perpendicular to the flow direction. The source is located at the brightest point of the jet. Like jets from low luminosity young stars, the HH 80/81 jet consists of a series of knots. The knots extend beyond the central region shown here, and the south-western lobe points directly towards HH 80 and 81. In the opposite direction, along the well defined flow axis, a radio counterpart to the visible HH objects is found; this object is hidden from view by a large molecular cloud. The total projected extent of this bipolar jet system exceeds 5 pc. The dynamical timescale for the system is likely to be short, because extremely high radial velocities, up to 700 km s^{-1}, were detected in HH 80/81 (Heathcote *et al.* 1998).

The case of the HH 80/81 jet system demonstrates that even massive young stars can produce highly collimated bipolar jets, which appear to be rather similar to those from low luminosity young stars, except for being much larger and faster, and probably also considerably more massive.

8. Theoretical models of HH objects

8.1. BASIC THEORETICAL IDEAS

A variety of mechanisms have over the years been proposed to explain the shock waves responsible for HH emission. Early models for the formation of shock waves in HH objects include the "spherical explosion" scenario (Böhm 1978) and the wind focussing mechanisms of Cantó (1980) and Königl (1982) (also studied by Cantó & Rodríguez 1980; Barral & Cantó 1981; Smith 1986; Cantó *et al.* 1986). In these models, the HH emission was assumed to be associated with the walls and tips of the elongated cavities produced in the wind focussing process.

These wind focussing models were also proposed as possible jet collimation mechanisms, the HH objects then being associated with the jet rather than with the wind cavity walls (Königl 1982; Cantó *et al.* 1988; Raga & Cantó 1989a,b; Kim & Raga 1991; somewhat related calculations also being carried out by Peter & Eichler 1996). The effect on the wind collimation due to the presence of an infalling envelope was also studied (Frank & Noriega-Crespo 1994; Frank & Mellema 1996; Mellema & Frank 1997; Wilkin & Stahler 1998). However, these wind focussing mechanisms are now less generally accepted than the MHD wind production/collimation models (see the review of Shu in these Proceedings).

One of the initial suggestions was that the HH knots were slowly moving condensations, embedded in a supersonic wind ejected from a young star. This "shocked cloudlet" model was initially suggested by Schwartz (1978), and then studied further by Schwartz & Dopita (1980), Raga & Wang (1994) and Raga *et al.* (1998a). An alternative "interstellar bullet" scenario (in which HH objects correspond to fast moving cloudlets embedded in a more or less stationary medium) was suggested by Norman & Silk (1979).

More recent models are based on the idea that the HH emission is associated with shock waves produced in a jet-like flow. Dopita *et al.* (1982b) made the initial suggestion that the emission of some HH objects could be the result of shock waves produced at the "head" or "working surface" of a jet-like flow. Following this idea, a considerable effort has been made to model HH objects in terms of a jet beam interacting with the surrounding environment. In these models, the production of the jet itself is not considered, assuming that it is a decoupled problem (see the paper of Shu in these Proceedings),

In the following subsections, we describe the efforts that have been made to model HH objects as plane or bow shocks (section 8.2), to describe them as working surfaces at the heads of jet (section 8.3), and the attempts to model jet-like HH objects in terms of stationary (section 8.4) or travelling (section 8.5) "crossing shocks". The possibly most favoured current model of knots as "internal working surfaces" is described in section 8.6. Finally, in section 8.7 we discuss the implications of current observations on the models of HH objects.

8.2. PLANE-PARALLEL AND BOW SHOCKS

Following the initial suggestion of Schwartz (1978), the emission of HH objects has since been modelled as the result of the excitation of gas by passing shock waves. The most simple problem that can be treated is of course the one of a stationary, plane-parallel shock wave, and quite detailed calculations of this problem (including detailed microphysical processes, as well as the transport of the diffuse, ionizing radiation) have been made in the context of HH objects.

Several papers give predictions of the atomic/ionic emission line fluxes of plane-parallel, stationary HH shocks (Dopita 1978; Raymond 1979; Shull & McKee 1979; Dopita *et al.* 1982a; Binette *et al.* 1985; Hartigan *et al.* 1987, 1994, 1995). The radio free-free continuum of such shocks was modelled by Curiel *et al.* (1987) and by Ghavamian & Hartigan (1998). Also, predictions of observed line fluxes were carried out for the plane-parallel, time-dependent case (Innes *et al.* 1987a,b,c; Gaetz *et al.* 1988; Gaetz 1990).

Given the fact that the "shocked cloudlet", "interstellar bullet" and "jet" models for HH objects (see section 8.1) all predict that at least part of the emission is formed in a bow shock, Hartmann & Raymond (1984) calculated the emission of such a bow shock using a superposition of plane-parallel shocks. This "quasi-1D" bow shock model approach was successfully used to obtain predictions of emission line ratios, line profiles, spatially resolved line profiles and narrow-band images of HH objects (Choe *et al.* 1985; Raga & Böhm 1985, 1986; Raga 1986; Raga *et al.* 1986; Hartigan *et al.* 1987, 1990; Noriega-Crespo *et al.* 1989, 1990; Morse *et al.* 1994; Indebetouw & Noriega-Crespo 1995). Such "quasi-1D" models have also been used to study the non-axisymmetric structures that result from the interaction of a jet with a non-uniform medium (Henney 1996), and to describe the kinematical properties of the proper motions of condensations in a bow shock flow (Raga *et al.* 1997a). Regrettably, the topic of preionization in a bow shock has received relatively little attention in the literature of HH objects (Raymond *et al.* 1988; Raga & Wang 1994).

The recent explosion in observational studies of H_2 emission in HH objects has motivated models of the molecular excitation in plane-parallel and bow shocks (Hartigan *et al.* 1989; Smith & Brand 1990a,b,c,d; Smith 1991; Smith *et al.* 1991a,b; Wolfire & Königl 1991, 1993). Interestingly, the issue of molecular excitation in HH objects is far from settled, and important questions remain regarding whether the molecular emission is produced in a magnetic or radiative precursor, or alternatively is the result of the excitation by a (very !) highly magnetized, sub-Alfvénic "C-shock".

It was already seen several years ago (and clearly more so in the recent HST results) that the "quasi-1D" bow shock models were insufficient for modelling spatially resolved observations of HH objects (Raga & Binette 1991). This result motivated the calculation of fully 2D, axisymmetric bow shocks (Raga & Böhm 1987; Raga *et al.* 1988, 1997b; Cantó & Raga 1998) produced by the interaction of a supersonic wind with a rigid obstacle. These models provided the first available dynamical explanation of the appearance of the condensations observed in HH bow shocks.

Finally, an interesting sideline in modelling the emission line profiles and images of HH bow shocks has been to consider the scattering of the direct emission on the surrounding, dusty environment (Calvet *et al.* 1992; Noriega-Crespo *et al.* 1991; Feldman & Raga 1991; Henney *et al.* 1994, 1995). These models have been successfully applied to modelling the line profiles of HH 1, and might have more important applications in the future, when more extended spectropolarimetric observations of HH objects become available. A second interesting topic that is becoming very important from the observational point of view is the formation of masers in outflows from young stars, and we are likely to see more theoretical work on this subject in the near future (see, e.g., Mac Low *et al.* 1994).

8.3. WORKING SURFACES

The next step in modelling HH objects has been to consider the real, two-shock structure of the working surface at the head of a jet. This structure is schematically shown in Fig. 14.

In the context of the highly radiative HH jets, the first numerical models of working surfaces in jets were the ones of Raga (1988) and Blondin *et al.* (1989, 1990). These models were used to obtain predictions of narrow-band, emission line maps. Also, Hartigan (1989) and Raga & Noriega-Crespo (1993) obtained predictions of the relative contributions to the observed line fluxes of the bow shock and Mach disk from plane-parallel shock models.

More sophisticated numerical simulations of HH jets were later carried out including a 3D description and/or a more realistic treatment of the

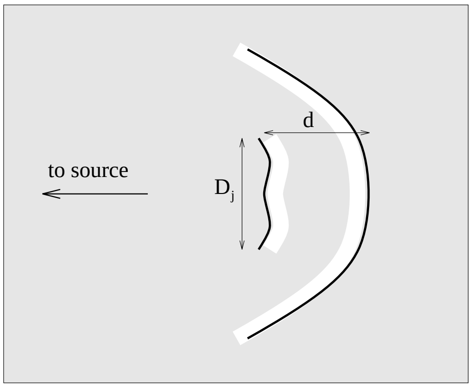

Figure 14. *Schematic diagram of a working surface in a jet flow. Such a shock structure is formed at the "head" of a jet (where the jet beam interacts directly with the undisturbed environment). Also, "internal working surfaces" can be formed in a jet ejected from a variable source as a result of the "catching up" of slower moving material by faster material ejected at later times. The working surface has two shocks : a Mach disk or "jet shock" (of diameter D_j) and a bow shock. For the case of strongly radiative HH jets, the expectation is that the separation d between the jet and bow shocks would satisfy the condition $d \ll D_j$. However, there are different possible alternatives for a working surface to violate this condition (see Cerqueira et al. 1997; Frank et al. 1998; Raga et al. 1998b), which can be invoked to model HH objects with large separations between the Mach disk and the bow shock.*

relevant microphysical processes (de Gouveia dal Pino & Benz 1993; Stone & Norman 1993). The effects of a stratified medium (Stone & Norman 1994; de Gouveia dal Pino *et al.* 1996; de Gouveia dal Pino & Birkinshaw 1996) and of a supersonic sidewind (Lim & Raga 1998) on radiative HH jets have been studied with 3D numerical simulations. Also, both analytic and numerical working surface models have been proposed to model the coupling between HH jets and the surrounding molecular outflows (Masson & Chernin 1993; Raga & Cabrit 1993; Chernin *et al.* 1994; Raga *et al.* 1995; Suttner *et al.* 1997).

In recent papers it has been shown that jet cross sections with centrally peaked ram pressure distributions (Raga *et al.* 1998b) or the presence of a toroidal magnetic field (Cerqueira *et al.* 1997; Frank *et al.* 1998) result in the formation of an axially extended cool "nose cone" separating the bow shock and the Mach disk. This prediction appears to have a clear application to the structures observed in the HST images of HH 47A.

Finally, an interesting aspect of HH jets has been the study of collisions of jets with dense clouds (Reipurth *et al.* 1996; Raga & Cantó 1995; Raga *et al.* 1996a). However, these collisions appear to be rare, and the calculations currently only have applications to HH 110 and possibly to HH 7-11.

8.4. STEADY JETS

It has been suggested that the knots along HH jets could be the result of stationary recollimation shocks (Falle *et al.* 1987; Cantó *et al.* 1989; Raga 1991; Raga *et al.* 1990b, 1991a; Biro *et al.* 1993) or MHD compression waves (Pelletier & Pudritz 1992; Bacciotti *et al.* 1997; Ouyed & Pudritz 1997a) formed within the jet beam. The theory of such stationary structures has been studied in detail, and both analytical and numerical descriptions have been obtained for the radiative, HH jet case, and detailed predictions of observable quantities have been made. Detailed studies have been carried out of the effects of the gravity of the central object (Fiege & Henriksen 1996a,b), of an environmental pressure gradient (Smith 1994b; Cantó & Raga 1996; Raga & Cantó 1996) and of the presence of a supersonic sidewind (Cantó & Raga 1995). Also, predictions of the observational properties of a steady jet launched by an MHD wind have been made (Shang *et al.* 1998).

The stationary recollimation shock models reproduce very well the knot structures that are produced in laboratory jets. However, the observation of high proper motions in many HH jets clearly indicates that the knots in HH objects are of a different origin from the knots seen in laboratory jets, and that they do not correspond to steady recollimation shocks or compression waves. Because of this fact, recent models of knots in HH jets have focussed on other mechanisms that do produce travelling knots.

8.5. INSTABILITIES IN JET BEAMS

There are several studies in which condensations in HH flows are modelled as being the result of thermal (de Gouveia dal Pino & Opher 1990), hydrodynamic (Silvestro *et al.* 1987; Massaglia *et al.* 1992; Stone *et al.* 1995, 1997; Hardee & Stone 1997; Rossi *et al.* 1997; Micono *et al.* 1998a,b; Downes 1998) or magnetohydrodynamic instabilities (Ouyed & Pudritz 1997b; Goodson *et al.* 1997; Frank *et al.* 1998) in a jet beam, which all produce travelling shock structures. The most detailed predictions of the observable properties of such instabilities are the hydrodynamic simulations of Micono *et al.* (1998b), who compute predicted emission line maps.

The work discussed above has focussed on the production of knot structures in jets as a result of instabilities. It has also been argued that hydrodynamic K-H instabilities in the jet beam might lead to the formation of a turbulent mixing layer (at the outer boundary of the beam) or to a fully turbulent jet (see Kahn 1980), both possibilities being important either for producing the optical/IR emission of HH jets or as coupling mechanisms between the jet and the surrounding molecular outflow (see the review of Bachiller in these Proceedings). Both the turbulent mixing layers and the fully turbulent regime have been modelled in terms of a "turbulent viscosity approach" (Cantó & Raga 1991; Richer *et al.* 1992; Raga *et al.* 1993b; Raymond *et al.* 1994; Stahler 1994; Taylor & Raga 1995; Raga *et al.* 1995; Noriega-Crespo *et al.* 1996), which leads to predictions of the observable properties of a spatially averaged "mean flow". The detailed spatial structure of the turbulent eddies is not modelled with this approach.

The remaining step in the study of hydrodynamic instabilities is to study the transition from the "coherent eddie" regime described by the numerical simulations to the "fully turbulent" regime described by the turbulent viscosity approach. In order to do this, 3D numerical simulations are necessary (as the 2D and 3D turbulent cascades have very different properties). We now see the first attempts to carry out this step for the case of adiabatic, extragalactic jets, and studies for the radiative, HH jet case will probably appear in the literature in the near future.

8.6. JETS FROM VARIABLE SOURCES

It was first suggested by Rees (1978), that a time-variability in the velocity with which the jet is ejected would result in the formation of shock waves travelling down the jet flow. This was studied numerically by Wilson (1984), who tried to model double-lobed radio sources in terms of jets resulting from two "outflow events". The first theoretical study of HH jets from variable sources appears to be the "pulsed jet" model of Choe & Henriksen (1986).

Raga *et al.* (1990a) argued that velocity time-variabilities of supersonic amplitude would result in the formation of two-shock "internal working surfaces" travelling down the jet beam, and that at least part of the emission observed in HH jets could correspond to such structures. This idea has been studied quite extensively both analytically (Kofman & Raga 1992; Raga & Kofman 1992; Raga & Noriega-Crespo 1992; Raga 1992; Raga & Cabrit 1993; Smith *et al.* 1997a) and numerically (Hartigan & Raymond 1993; Stone & Norman 1993; Falle & Raga 1993, 1995; de Gouveia dal Pino & Benz 1994; Biro & Raga 1994; Biro 1996; Suttner *et al.* 1997; Smith *et al.* 1997b) with specific application to HH jets and molecular outflows.

The formation of working surfaces in a variable ejection velocity jet is an intuitively simple process. During the periods in which the ejection velocity is growing as a function of time, one produces a situation in which the faster material ejected at later times "catches up" with the slower material ejected earlier. This "catching up" occurs at a finite distance x_c from the source, which is given by the expression :

$$x_c = \left(\frac{{u_0}^2}{du_0/d\tau} \right)_{min} , \tag{1}$$

where $u_0(\tau)$ is the ejection velocity (as a function of the time τ at which the flow is ejected), and the minimum is obtained over the period of the ejection velocity variability.

For distances larger than x_c, an internal working surface is formed (see Fig. 14). This working surface then travels down the jet flow. Initially, the strength of the shocks of the working surface grow with increasing x, then reach a maximum, and eventually decay monotonically as the working surface travels away from the source.

If one allows the source to have an ejection velocity variability that can be described by a superposition of sinusoidal modes, it is possible to obtain complex morphologies. In order to understand the effects of such a multi-mode variability, one can rewrite eq. (1) in the approximate way :

$$x_{c,a} \approx \frac{\overline{v}^2 \tau_a}{2 v_a} \,, \tag{2}$$

where $x_{c,a}$ is the distance from the source at which the working surfaces of the mode with period τ_a and (full) amplitude v_a are formed. In this equation, $\overline{v}$ is the mean velocity of the time-dependent ejection velocity. From equation (2), we then see that for a fixed amplitude, the larger period modes form working surfaces at increasing distances from the source.

The working surfaces for the different modes are formed at a distance $x_{c,a}$ given (in an approximate way) by equation (2). The shocks associated with the working surface first grow in strength, peak at a distance $x_{m,a} \approx \pi x_{c,a}/2$, and then decay for larger distances from the source (with shock velocities following a $v_s \propto 1/x$ law, see Raga & Kofman 1992).

The different modes of a variable ejection velocity have an interesting interaction. The long period modes produce a modulation of the amplitude of the short period modes, resulting in the production of "trains" of short period knots travelling down the jet beam. This mechanism has been proposed by Raga & Noriega-Crespo (1998) to explain the chains of knots observed in some HH jets. In the following section, this work is described in more detail.

Finally, the effect of a time-variability in the ejection direction of HH jets has also been studied (Raga *et al.* 1993a; Biro *et al.* 1995; Cliffe *et al.* 1996). Furthermore, a general velocity+direction time variability has been suggested as a mechanism to convert an HH jet into a series of disconnected "bullets" (Raga & Biro 1993; Suttner *et al.* 1997). A detailed study of the application of these models to actual HH jets still remains to be done.

8.7. COMPARING MODELS AND OBSERVATIONS OF HH JETS

Most of the comparisons between observations of HH objects and theoretical models have been limited to analyses based either on plane-parallel shock or on bow shock models (see, e.g., Solf *et al.* 1986; Hartigan *et al.* 1987; Raga *et al.* 1986). Comparisons with bow shock models of observed line ratios, line profiles, spatially resolved line profiles and narrow band images have been carried out.

Interestingly, more advanced models have mostly been used only for carrying out purely qualitative comparisons with observations. For example, it has been shown that both models from variable sources as well as models of K-H instability modes can produce knots that qualitatively resemble the knots along HH jets (in the sense that predicted Hα emission line maps do show a series of aligned knots).

It has been pointed out that objects that show knots with a strong jet to counter-jet symmetry probably are the result of a source variability, since there is no reason to expect that Kelvin-Helmholtz modes (arising from instabilities in the jet beam/environment boundary) would show such a symmetry (Gredel & Reipurth 1994, Zinnecker *et al.* 1998). However, the converse argument (i.e., that asymmetric jet/counterjet systems have to be the result of Kelvin-Helmholtz modes) does not necessarily follow, since the propagation of internal working surfaces could be strongly affected by the existence of differences in the properties of the environments surrounding the jet and the counterjet. This, however, is a topic that has not yet been explored in a detailed way.

Recently, Raga & Noriega-Crespo (1998) have used analytic considerations to derive parameters for a multimode variability that could explain the observed proper motions of the knots along the HH 34 jet. The Hα intensity maps predicted from a numerical simulation (computed with the derived parameters) are shown in Fig. 15. It is clear that the predicted intensity maps do show a strong resemblance to the morphology and intensities observed for the knots along the HH 34 jet.

In the future, more efforts will have to be made to attempt to reproduce the kinematical properties, line ratios, and morphologies (particularly, the high resolution maps obtained with HST) of different HH jets. The best candidates for such studies are of course the objects that show the more organized spatial structures (e.g., HH 34, 111, 211, 212, 228), as these structures might be easier to model than the more complex and chaotic structures observed in other HH objects.

Even though the more promising model for HH jets at this time appears to be the "internal working surface" model, important questions still need to be answered. For example :

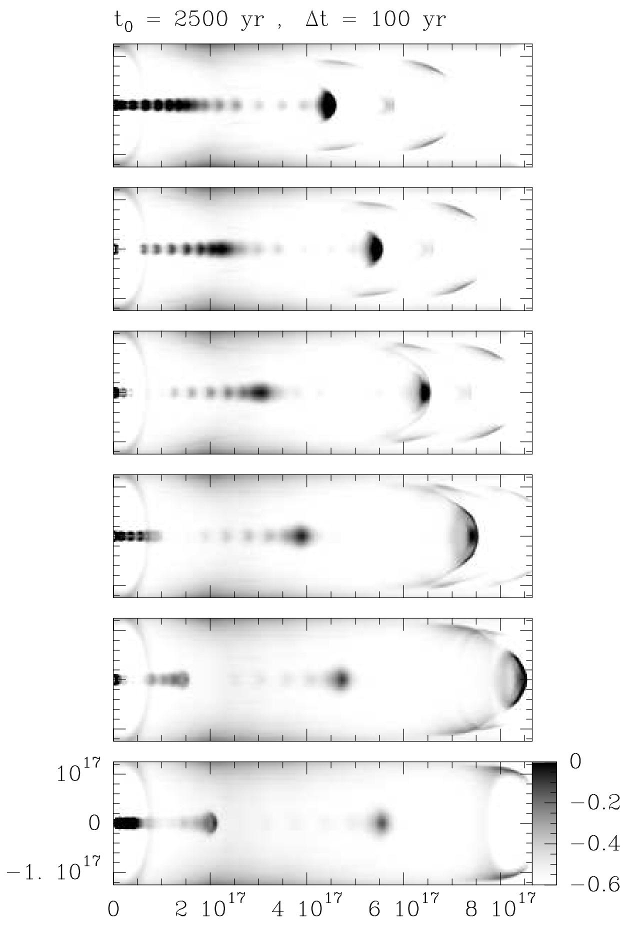

Figure 15. Time sequence of Hα intensity maps obtained from a three-mode, variable ejection velocity model of HH 34 (from Raga & Noriega-Crespo 1998). The jet is ejected with a velocity variability with three sinusoidal modes (with half-amplitudes of 70, 40 and 15 km/s, and periods of 1200, 310 and 27 years, respectively) chosen so as to reproduce the present-day structure of the HH 34 jet. The Hα maps have been calculated assuming an angle of 30° *between the outflow axis and the plane of the sky. The top frame corresponds to an integration time of 2500 yr, and the following frames correspond to time-intervals of 100 yr. The greyscale is a logarithmic representation of the Hα intensity (the relative scale, normalized to the peak of the t=2900 yr panel, is shown in the wedge to the right of the lower frame).*

- can variable velocity jet models explain the spatial distribution of emitting knots in different HH jets (this has only been attempted for HH 34, see above) ?

- can the interaction with the surrounding environment modify the properties of internal working surfaces, or do knots in asymmetric jet/counterjets require a different interpretation (e.g., K-H modes) ?

- what are the detailed consequences of the presence of a stratified environment and/or motion of the source ?

Finally, an important problem in modelling HH objects is the interpretation of the emission line ratios. Though the observed line ratios were the inspiration that initially led Schwartz (1978) to suggest that the emission of HH objects was excited by the passage of shock waves, the detailed modelling of these line ratios has proved to be more difficult than expected. Some of the problems encountered are summarized by Raga *et al.* (1996b), and are described in many papers in the literature.

9. References

Ambartsumian, V.A. 1947, *Stellar Evolution and Astrophysics* (Yerevan, Acad. Sci. Armenian SSR.)
Ambartsumian, V.A. 1954, *Comm. Byurakan Obs.* No. 13
Axon, D.J., Taylor, K. 1984, *MNRAS* 207, 241
Bacciotti, F., Chiuderi, C., Oliva, E. 1995, *A&A* 296, 185
Bacciotti, F., Chiuderi, C., Pouquet, A. 1997, *ApJ* 478, 594
Bally, J., Devine, D. 1994, *ApJ* 428, L65
Bally, J., Devine, D., Fesen, R., Lane, A. 1995, *ApJ* 454, 345
Bally, J., Devine, D., Reipurth, B. 1996, *ApJ* 473, L49
Barral, J. F., Cantó, J. 1981, *RMxAA* 5, 101
Beckwith, S., Gatley, I., Matthews, K., Neugebauer, G. 1978, *ApJ* 223, L41
Binette, L., Dopita, M. A., Tuohy, I. R. 1985,*ApJ* 297, 476
Biro, S. 1996, *MNRAS* 278, 990
Biro, S., Raga, A. C. 1994, *ApJ* 434, 221
Biro, S., Cantó, J., Raga, A. C., Binette, L. 1993, *RMxAA* 25, 95
Biro, S., Raga, A. C., Cantó, J. 1995, *MNRAS* 275, 557
Blondin, J. M., Fryxell, B. A., Königl, A. 1990, *ApJ* 360, 370
Blondin, J. M., Königl, A., Fryxell, B. A. 1989, *ApJ* 337, L37
Böhm, K.H. 1956, *ApJ* 123, 379
Böhm, K. H. 1978, *A&A* 64, 115
Böhm, K.H. 1983, *Rev. Mex. Astron. Astrofis.* 7, 55
Böhm, K.H. 1990, in *Structure and Dynamics of the Interstellar Medium*, eds. G. Tenorio-Tagle, M. Moles, J. Melnick, Springer, p. 282
Böhm, K.H., Böhm-Vitense, E. 1984, *ApJ* 277, 216
Böhm, K.H., Raga, A.C. 1987, *PASP* 99, 265
Böhm, K.H., Solf, J. 1990, *ApJ* 348, 297
Böhm, K.H., Goodson, A.P. 1997, in *Herbig-Haro Flows and the Birth of Low Mass Stars*, IAU Symp. No. 182, Eds. Bo Reipurth & C. Bertout, p.47
Böhm, K.H., Perry, J.F., Schwartz, R.D. 1973, *ApJ* 179, 149
Böhm, K.H., Schwartz, R.D., Siegmund, W.A. 1974, *ApJ* 193, 353
Böhm, K.H., Brugel, E.W., Mannery, E. 1980, *ApJ* 235, L137
Böhm, K.H., Böhm-Vitense, E., Brugel, E.W. 1981, *ApJ* 245, L113
Böhm, K.H., Brugel, E.W., Olmsted, E. 1983, *A&A* 125, 23
Böhm, K.H., Bührke, Th., Raga, A.C., Brugel, E.W., Witt, A.N., Mundt, R. 1987, *ApJ* 316, 349

Böhm, K.H., Raga, A.C., Binette, L. 1991, *PASP* 103, 85
Böhm, K.H., Noriega-Crespo, A., Solf, J. 1993, *ApJ* 416, 647
Böhm-Vitense, E., Böhm, K.H., Cardelli, J.A., Nemec, J.M. 1982, *ApJ* 262, 224
Brown, A., Jordan, C., Millar, T.J., Gondhalekar, P., Wilson, R. 1981, *Nature* 290, 34
Brugel, E.W., Böhm, K.H., Mannery, E. 1981a, *ApJS* 47, 117
Brugel, E.W., Böhm, K.H., Mannery, E. 1981b, *ApJ* 243, 874
Brugel, E.W., Shull, J.M., Seab, C.G. 1982, *ApJ* 262, L35
Brugel, E.W., Böhm, K.H., Shull, J.M., Böhm-Vitense, E. 1985, *ApJ* 292, L75
Bührke, T., Mundt, R., Ray, T.P. 1988, *A&A* 200, 99
Calvet, N., Cantó, J., Binette, L., Raga, A. C. 1992, *RMxAA* 24, 81
Cameron, M., Liseau, R. 1990, *A&A* 240, 409
Cantó, J. 1980, *A&A* 86, 327
Cantó, J., Rodríguez, L. F. 1980, *ApJ* 239, 982
Cantó, J., Raga, A. C. 1991, *ApJ* 372, 646
Cantó, J., Raga, A. C. 1995, *MNRAS* 227, 1120
Cantó, J., Raga, A. C. 1996, *MNRAS* 280, 559
Cantó, J., Raga, A. C. 1998, *MNRAS* 297, 383
Cantó, J., Raga, A. C., Binette, L. 1989, *RMxAA* 17, 65
Cantó, J., Sarmiento, A., Rodríguez, L. F. 1986, *RMxAA* 13, 107
Cantó, J., Tenorio-Tagle, G. Różyczka, M. 1988, *A&A* 192, 287
Carr, J.S. 1993, *ApJ* 406, 553
Cerqueira, A. H., de Gouveia dal Pino, E. M., Herant, M. 1997, *ApJ* 489, L185
Charnley, S. B., Dyson, J. E., Hartquist, T. W., Williams, D.A. 1988, *MNRAS* 235, 1257
Chernin, L., Masson, C., de Gouveia dal Pino, E., Benz, W. 1994, *ApJ* 426, 204
Chevalier, R.A., Raymond, J.C. 1978, *ApJ* 225, L27
Choe, S.U., Böhm, K.H., Solf, J. 1985, *ApJ* 288, 338
Choe, S. U., Henriksen, R. N, 1986, *ApJ* 305, 131
Cliffe, J. A., Frank, A., Jones, T. W. 1996, *MNRAS* 282, 1114
Corcoran, M., Ray, T.P. 1998, *A&A* 336, 535
Curiel, S., Cantó, J., Rodríguez, L. F. 1987, *RMxAA* 14, 595
Davis, C.J., Eislöffel, J., Ray, T.P. 1994, *ApJ* 426, L93
Devine, D., Bally, J., Reipurth, B., Heathcote, S. 1997, *AJ* 114, 2095
Devine, D., Bally, J., Reipurth, B., Shepherd, D., Watson, A. 1999, *AJ* in press
Dopita, M.A. 1978, *ApJS* 37, 117
Dopita, M.A., Binette, L., Schwartz, R.D. 1982a, *ApJ* 261, 183
Dopita, M.A., Schwartz, R.D., Evans, I. 1982b, *ApJ* 263, L73
Downes, T. P. 1998, *A&A* 331, 1130
Eislöffel, J., Mundt, R. 1994, *A&A* 284, 530
Eislöffel, J., Mundt, R., Böhm, K.-H. 1994a, *AJ* 108, 1042
Eislöffel, J., Davis, C.J., Ray, T.P., Mundt, R. 1994b, *ApJ* 422, L91
Elias, J.H. 1980, *ApJ* 241, 728
Falle, S. A. E. G., Raga, A. C. 1993, *MNRAS* 261, 573
Falle, S. A. E. G., Raga, A. C. 1995, *MNRAS* 272, 785
Falle, S. A. E. G., Innes, D. E., Wilson, M. J. 1987, *MNRAS* 225, 741
Feldman, H. A., Raga, A. C. 1991, *AJ* 102, 2049
Fiege, J. D., Henriksen, R. N. 1996s, *MNRAS* 281, 1038
Fiege, J. D., Henriksen, R. N. 1996b, *MNRAS* 281, 1055
Frank, A., Noriega-Crespo, A. 1994, *A&A* 290, 643

Frank, A., Mellema, G. 1996, *ApJ* 472, 684
Frank, A., Ryu, D., Jones, T. W., Noriega-Crespo, A. 1998, *ApJ* 494, L79
Gaetz, T. J. 1990, *ApJ* 353, 357
Gaetz, T. J., Edgar, R. J., Chevalier, R. A. 1988, *ApJ* 329, 927
Ghavamian, P., Hartigan, P. 1998, *ApJ* 501, 687
Goodson, A. P., Winglee, R. M., Böhm, K. H. 1997, *ApJ* 489, 199
de Gouveia dal Pino, E. M., Opher, R. 1990, *A&A* 231, 571
de Gouveia dal Pino, E. M., Benz, W. 1993, *ApJ* 410, 686
de Gouveia dal Pino, E. M., Benz, W. 1994, *ApJ* 435, 261
de Gouveia dal Pino, E. M., Birkinshaw, M. 1996, *ApJ* 471, 832
de Gouveia dal Pino, E. M., Birkinshaw, M., Benz, W. 1996, *ApJ* 460, L111
Graham, J.A., Elias, J.H. 1983, *ApJ* 272, 615
Gredel, R. 1994, *A&A* 292, 580
Gredel, R., Reipurth, B. 1994, *A&A* 289, L19
Hardee, P. E., Stone, J. M. 1997, *ApJ* 483, 136
Haro, G. 1952, *ApJ* 115, 572
Haro, G. 1953, *ApJ* 117, 73
Haro, G., Minkowski, R. 1960, *AJ* 65, 490
Hartigan, P. 1989, *ApJ* 339, 987
Hartigan, P., Raymond, J. C. 1993, *ApJ* 409, 705
Hartigan, P., Raymond, J., Hartmann, L. 1987, *ApJ* 316, 323
Hartigan, P., Curiel, S., Raymond, J. 1989, *ApJ* 347, L31
Hartigan, P., Raymond, J., Meaburn, J. 1990, *ApJ* 362, 624
Hartigan, P., Morse, J. A., Raymond, J. C. 1994, *ApJ* 436, 125
Hartigan, P., Morse, J. A., Raymond, J. C. 1995, *ApJ* 444, 943
Hartigan, P., Morse, J., Tumlinson, J., Raymond, J., Heathcote, S. 1999, *ApJ* in press
Hartmann, L., Raymond, J. 1984, *ApJ* 276, 560
Heathcote, S., Reipurth, B. 1992, *AJ* 104, 2193
Heathcote, S., Morse, J.A., Hartigan, P., Reipurth, B., Schwartz, R.D., Bally, J., Stone, J.M. 1996, *AJ* 112, 1141
Heathcote, S., Reipurth, B., Raga, A.C. 1998, *AJ* 116, 1940
Henney, W. J. 1996, *RMxAA* 32, 3
Henney, W. J., Raga, A. C., Axon, D. J. 1994, *ApJ* 427, 305
Henney, W. J., Axon, D. J. 1995, *ApJ* 454, 233
Herbig, G.H. 1950, *ApJ* 111, 11
Herbig, G.H. 1951, *ApJ* 113, 697
Herbig, G.H. 1952, *J.R. Astron. Soc. Can.* 46, 222
Herbig, G.H., Jones, B.F. 1981, *AJ* 86, 1232
Herbig, G.H., Jones, B.F. 1983, *AJ* 88, 1040
Hirth, G.A., Mundt, R., Solf, J. 1994, *ApJ* 427, L99
Indebetouw, R., Noriega-Crespo, A. 1995, *AJ* 109, 752
Innes, D. E., Giddings, J. R., Falle, S. A. E. G. 1987a, *MNRAS* 224, 179
Innes, D. E., Giddings, J. R., Falle, S. A. E. G., 1987b, *MNRAS* 226, 67
Innes, D. E., Giddings, J. R., Falle, S. A. E. G., 1987c, *MNRAS* 227, 1021
Joy, A.H. 1942, *PASP* 54, 15
Kahn, F. D. 1980, *A&A* 83, 303
Kim, S.-H., Raga, A. C. 1991, *ApJ* 379, 689
Kofman, A. C., Raga, A. C. 1992, *ApJ* 390, 359
Königl, A. 1982, *ApJ* 261, 115

Lada, C.J. 1987, in IAU Symp. no. 115 *Star Forming Regions*, eds. M. Peimbert, J. Jugaku (Reidel), p. 1
Lim, A. J., Raga, A. C. 1998, *MNRAS* 298, 871
Liseau, R., Huldtgren, M., Fridlund, C.V.M., Cameron, M. 1996, *A&A* 306, 255
Mac Low, M. M., Elitzur, M., Stone, J. M., Königl, A. 1994, *ApJ* 427, 914
Martí, J., Rodríguez, L.F., Reipurth, B. 1993, *ApJ* 416, 208
Martí, J., Rodríguez, L.F., Reipurth, B. 1995, *ApJ* 449, 268
Martí, J., Rodríguez, L.F., Reipurth, B. 1998, *ApJ* 502, 337
Massaglia, S., Trussoni, E., Bodo, G., Rossi, P., Ferrari, A. 1992, *A&A* 260, 243
Masson, C., Chernin, L. 1993, *ApJ* 414, 230
Meaburn, J., Dyson, J. 1987, *MNRAS* 225, 863
Mellema, G., Frank, A. 1997, *MNRAS* 292, 795
Micono, M., Massaglia, S., Bodo, G., Rossi, P., Ferrari, A. 1998a, *A&A* 333, 989
Micono, M., Massaglia, S., Bodo, G., Rossi, P., Ferrari, A. 1998b, *A&A* 333, 1001
Miller, J.S. 1968, *ApJ* 154, L57
Morse, J. A., Hartigan, P., Heathcote, S., Raymond, J. C., Cecil, G. 1994, *ApJ* 425, 738
Mundt, R., Fried, J.W. 1983, *ApJ* 274, L83
Mundt, R., Stocke, J., Stockman, S. 1983, *ApJ* 265, L71
Mundt, R., Bührke, T., Fried, J.W., Neckel, T., Sarcander, M., Stocke, J. 1984, *A&A* 140, 17
Mundt, R., Brugel, E.W., Bührke, T. 1987, *ApJ* 319, 275
Mundt, R., Ray, T.P., Bührke, T., Raga, A.C., Solf, J. 1990, *A&A* 232, 37
Mundt, R., Ray, T.P., Raga, A.C. 1991, *A&A* 252, 740
Noriega-Crespo, A., Böhm, K. H., Raga, A. C. 1989, *AJ* 98, 1388
Noriega-Crespo, A., Böhm, K. H., Raga, A. C. 1990, *AJ* 99, 1918
Noriega-Crespo, A., Böhm, K. H., Calvet, N. 1991, *ApJ* 379, 676
Noriega-Crespo, A., Garnavich, P. M., Raga, A. C., Cantó, J., Böhm, K. H. 1996, *ApJ* 462, 804
Norman, C., Silk, J. 1979, *ApJ* 228, 197
Ogura, K., Walsh, J. 1992, *ApJ* 400, 248
Ortolani, S., D'Odorico, S. 1980, *A&A* 83, L8
Osterbrock, D.E. 1958, *PASP* 70, 399
Ouyed, R., Pudritz, R. E. 1997a, *ApJ* 482, 712
Ouyed, R., Pudritz, R. E. 1997b, *ApJ* 484, 794
Pelletier, G., Pudritz, R. E. 1992, *ApJ* 394, 117
Peter, W., Eichler, D. 1996, *ApJ* 466, 840
Poetzel, R., Mundt, R., Ray, T.P. 1992, *A&A* 262, 229
Raga, A. C. 1986, *AJ* 92, 637
Raga, A. C. 1988, *ApJ* 335, 820
Raga, A. C. 1991, *AJ* 101, 1472
Raga, A. C. 1992, *MNRAS* 258, 301
Raga, A.C., Böhm, K.H. 1985, *ApJS* 58, 201
Raga, A.C., Böhm, K.H. 1986, *ApJ* 308, 829
Raga, A.C., Böhm, K.H. 1987, *ApJ* 323, 193
Raga, A.C., Mateo, M. 1987, *AJ* 94, 684
Raga, A.C., Mateo, M. 1988, *AJ* 95, 543
Raga, A. C., Cantó, J. 1989a, *ApJ* 344, 404
Raga, A. C., Cantó, J. 1989b, *PASP* 101, 1151
Raga, A. C., Binette, L. 1991, *RMxAA* 22, 265

Raga, A. C., Kofman, L. 1992, *ApJ* 386, 222
Raga, A. C., Noriega-Crespo, A. 1992, *RMxAA* 24, 9
Raga, A. C., Noriega-Crespo, A. 1993, *RMxAA* 25, 149
Raga, A. C., Biro, S. 1993, *MNRAS* 264, 758
Raga, A.C., Cabrit, S. 1993, *A&A* 278, 267
Raga, A. C., Wang, L. 1994, *MNRAS* 268, 354.
Raga, A. C., Cantó, J. 1995, *RMxAA* 31, 51
Raga, A. C., Cantó, J. 1996, *MNRAS* 280, 567
Raga, A. C., Noriega-Crespo, A. 1998, *AJ* 116, 2943
Raga, A.C., Böhm, K.H., Solf, J. 1986, *AJ* 92, 119
Raga, A.C., Mateo, M., Böhm, K.H., Solf, J. 1988, *AJ* 95, 1783
Raga, A.C., Cantó, J., Binette, L., Calvet, N. 1990a, *ApJ* 364, 601
Raga, A.C., Binette, L., Cantó, J. 1990b, *ApJ* 360, 612
Raga, A. C., Biro, S., Cantó, J., Binette, L. 1991a, *RMxAA* 22, 243
Raga, A.C., Mundt, R., Ray, T.P. 1991b, *A&A* 252, 733
Raga, A. C., Cantó, J., Biro, S. 1993a, *MNRAS* 260, 163
Raga, A. C., Cantó, J., Calvet, N., Rodríguez, L. F., Torrelles, J. M. 1993b, *A&A* 276, 539
Raga, A. C., Cabrit, S., Cantó, J. 1995a, *MNRAS* 273, 422
Raga, A. C., Taylor, S. D., Cabrit, S., Biro, S. 1995b, *A&A* 296, 833
Raga, A. C., Böhm, K. H., Cantó, J. 1996a, *RMxAA* 32, 161
Raga, A. C., Cantó, J., Steffen, W. 1996b, *QJRAS* 37, 493
Raga, A. C., Cantó, J., Curiel, S., Noriega-Crespo, A., Raymond, J. C. 1997a, *RMxAA* 33, 157
Raga, A. C., Mellema, G., Lundqvist, P. 1997b, *ApJS* 109, 517
Raga, A. C., Cantó, J., Curiel, S., Taylor, S. 1998a, *MNRAS* 295, 738
Raga, A. C., Cantó, J., Cabrit, S. 1998b, *A&A* 332, 714
Ray, T.P., Poetzel, R., Solf, J., Mundt, R. 1990, *ApJ* 357, L45
Raymond, J.C. 1979, *ApJS* 39, 1
Raymond, J. C., Hartmann, L., Hartigan, P. 1988, *ApJ* 326, 323
Raymond, J. C., Morse, J. A., Hartigan, P., Curiel, S., Heathcote, S. 1994, *ApJ* 434, 232
Rees, M. J. 1978, *MNRAS* 184, 61
Reipurth, B. 1989a, *Nature* 340, 42
Reipurth, B. 1989b, *A&A* 220, 249
Reipurth, B., Graham, J.A. 1988, *A&A* 202, 219
Reipurth, B., Heathcote, S. 1991, *A&A* 246, 511
Reipurth, B., Olberg, M. 1991, *A&A* 246, 535
Reipurth, B., Heathcote, S. 1997, in IAU Symp. No. 182 *Herbig-Haro Flows and the Birth of Low Mass Stars*, Eds. Bo Reipurth & C. Bertout, p. 3
Reipurth, B., Bally, J., Graham, J., Lane, A., Zealey, W. 1986, *A&A* 164, 51
Reipurth, B., Raga, A.C., Heathcote, S. 1992, *ApJ* 392, 145
Reipurth, B., Raga, A.C., Heathcote, S. 1996, *A&A* 311, 989
Reipurth, B., Hartigan, P., Heathcote, S., Morse, J., Bally, J. 1997a, *AJ* 114, 757
Reipurth, B., Bally, J., Devine, D. 1997b, *AJ* 114, 2708
Reipurth, B, Bally, J., Fesen, R., Devine, D. 1998a, *Nature* 396, 343
Reipurth, B., Devine, D., Bally, J. 1998b, *AJ* 116, 1396
Richer, J. S., Hills, R. E., Padman, R. 1992, *MNRAS* 254, 525
Rodríguez, L.F., Reipurth, B. 1989, *Rev. Mex. Astron. Astrofis.* 17, 59
Rodríguez, L.F., Reipurth, B. 1994, *A&A* 281, 882

Rodríguez, L.F., Moran, J.M., Ho, P.T.P., Gottlieb, E.W. 1980, *ApJ* 235, 845
Rossi, P., Bodo, G., Massaglia, S., Ferrari, A. 1997, *A&A* 321, 672
Schwartz, R.D. 1975, *ApJ* 195, 631
Schwartz, R.D. 1978, *ApJ* 223, 884
Schwartz, R.D. 1983, *ApJ* 268, L37
Schwartz, R. D., Dopita, M. A. 1980, *ApJ* 236, 543
Schwartz, R.D., Dopita, M.A., Cohen, M. 1985, *AJ* 90, 1820
Schwartz, R.D., Williams, P.M., Cohen, M., Jennings, D.G. 1988, *ApJ* 334, L99
Schwartz, R.D., Schultz, A.S.B., Cohen, M., Williams, P.M. 1995, *ApJ* 446, 318
Shang, H., Shu, F. H., Glassgold, A. E. 1998, *ApJ* 439, L91
Shull, J. M., McKee, C. F. 1979, *ApJ* 227, 131
Silvestro, G., Ferrari, A., Rosner, R., Trussoni, E., Tsinganos, K. 1987, *Nature* 325, 228
Smith, M. D. 1986, *MNRAS* 223, 57
Smith, M. D. 1991, *MNRAS* 252, 378
Smith, M.D. 1993, *ApJ* 406, 520
Smith, M.D. 1994a, *MNRAS* 266, 238
Smith, M. D. 1994b, *ApJ* 421, 400
Smith, M. D., Brand, P., 1990a, *MNRAS* 242, 495
Smith, M. D., Brand, P., 1990b, *MNRAS* 243, 498
Smith, M. D., Brand, P., 1990c, *MNRAS* 244, 384
Smith, M. D., Brand, P., 1990d, *MNRAS* 245, 108
Smith, M. D., Brand, P., Moorhouse, A. 1991a, *MNRAS* 248, 451
Smith, M. D., Brand, P., Moorhouse, A. 1991b, *MNRAS* 248, 730
Smith, M. D., Suttner, G., Zinnecker, H. 1997a, *A&A* 320, 325
Smith, M. D., Suttner, G., Yorke, H. W. 1997b, *A&A* 323, 223
Solf, J. 1987, *A&A* 184, 322
Solf, J., Böhm, K.H. 1987, *AJ* 93, 1172
Solf, J., Böhm, K.H. 1991, *ApJ* 375, 618
Solf, J., Böhm, K.H. 1993, *ApJ* 410, L31
Solf, J., Böhm, K.H., Raga, A.C. 1986, *ApJ* 305, 795
Solf, J., Böhm, K.H., Raga, A.C. 1988, *ApJ* 334, 229
Stahler, S. W. 1994, *ApJ* 422, 616
Stone, J. M., Norman, M. L. 1993a, *ApJ* 413, 198
Stone, J. M., Norman, M. L. 1993b, *ApJ* 413, 210
Stone, J. M., Norman, M. L. 1994, *ApJ* 420, 237
Stone, J. M., Xu, J., Mundy, L. G. 1995, *Nature* 377, 315
Stone, J. M., Xu, J., Hardee, P. E. 1997, *ApJ* 483, 136
Suttner, G., Smith, M. D., Yorke, H. W., Zinnecker, H. 1997, *A&A* 318, 595
Taylor, S. D., Raga, A. C. 1995, *A&A* 296, 823
Wilkin, F. P., Stahler, S. W. 1998, *ApJ* 502, 661
Wilson, M. J. 1984, *MNRAS* 209, 923
Wolfire, M. G., Königl, A. 1993, *ApJ* 415, 204
Wolfire, M. G., Königl, A. 1991, *ApJ* 383, 205
Yamashita, T., Suzuki, H., Kaifu, N., Tamura, M., Mountain, C.M., Moore, T.J.T. 1989, *ApJ* 347, 894
Zealey, W., Williams, P., Sandell, G., Taylor, K., Ray, T. 1992, *A&A* 262, 570
Zinnecker, H., Mundt, R., Geballe, T.R., Zealey, W.J. 1989, *ApJ* 342, 337
Zinnecker, H., McCaughrean, M., Rayner, J. 1998, *Nature* 394, 862